Association of the Arabidopsis oleoyl Δ12-desaturase FAD2 with pre-*cis*-Golgi stacks at endoplasmic reticulum-Golgi-exit sites

Larissa Launhardt[1], Johanna Uhlenberg[1], Hagen Stellmach[2], Marie Schomburg[1], Bettina Hause[2], Ingo Heilmann[1] and Mareike Heilmann[1,*] iD

[1]*Department of Plant Biochemistry, Institute of Biochemistry, Martin-Luther-University Halle-Wittenberg, 06120 Halle (Saale), Germany, and*
[2]*Department of Cell and Metabolic Biology, Leibniz Institute of Plant Biochemistry, 06120 Halle (Saale), Germany*

SUMMARY

The unsaturation of phospholipids influences the function of membranes. In *Arabidopsis thaliana*, the oleoyl Δ12-desaturase FAD2 converts oleic ($18:1^{\Delta9}$) to linoleic acid ($18:2^{\Delta9,12}$) and influences phospholipid unsaturation in different cellular membranes. Despite its importance, the precise localization of Arabidopsis FAD2 has not been unambiguously described. As FAD2 is thought to modify phospholipid-associated fatty acids at the endoplasmic reticulum (ER), from where unsaturates are distributed to other cellular sites, we hypothesized that FAD2 locates to ER subdomains enabling trafficking of lipid intermediates through the secretory pathway. Fluorescent FAD2 fusions used to test this hypothesis were first assessed for functionality by heterologous expression in yeast (*Saccharomyces cerevisiae*), and *in planta* by Arabidopsis *fad2* mutant rescue upon ectopic expression from an intrinsic *FAD2* promoter fragment. Light sheet fluorescence, laser scanning confocal or spinning disc microscopy of roots, leaves, or mesophyll protoplasts showed the functional fluorescence-tagged FAD2 variants in flattened donut-shaped structures of ~0.5–1 μm diameter, in a pattern not resembling mere ER association. High-resolution imaging of coexpressed organellar markers showed fluorescence-tagged FAD2 in a ring-shaped pattern surrounding ER-proximal Golgi particles, colocalizing with pre-*cis*-Golgi markers. This localization required the unusual C-terminal retention signal of FAD2, and deletion or substitutions in this protein region resulted in relaxed distribution and diffuse association with the ER. The distinct association of FAD2 with pre-*cis*-Golgi stacks in Arabidopsis root and leaf tissue is consistent with a contribution of FAD2 to membrane lipid homeostasis through the secretory pathway, as verified by an increased plasma membrane liquid phase order in the *fad2* mutant.

Keywords: lipid unsaturation, ER-subdomains, plasma membrane, secretory pathway, *Arabidopsis thaliana*, high-resolution live imaging, lightsheet microscopy.

INTRODUCTION

The biological function of cellular membranes depends on various factors, including the nature of the constituting membrane lipids. Plant membranes contain a mixture of amphipathic lipids, such as glycerophospholipids, glyceroglycolipids, or sphingolipids, which are required for bilayer formation (Horton et al., 2006). The degree of unsaturation in bilayer-forming lipids influences membrane fluidity and thereby the optimal function of intrinsic membrane processes, such as membrane transport. Membrane lipid unsaturation is also important for dynamic membrane processes, such as budding and fusion during trafficking, thereby influencing secretion and endocytosis as well as the homeostasis of integral membrane proteins. Moreover, membrane lipid unsaturation is also important for the integrity of membranes under changing environmental conditions, such as temperature or osmotic potential (Horton et al., 2006).

The fatty acid moieties of glycerolipids are desaturated by fatty acid desaturases (FADs) (Somerville et al., 2000). With the exception of the plastidial soluble stearoyl-ACP desaturase, FADs found in higher plants are thought to modify fatty acids esterified in membrane lipids, such as phosphatidylcholine (PC) at the endoplasmic reticulum (ER) or monogalactosyldiacylglycerol (MGDG) in plastids (Somerville et al., 2000). Enzymes of the FAD superfamily also

include fatty acid hydroxylases, epoxidases, or conjugases (Broadwater et al., 2002; Shanklin & Cahoon, 1998), which are all membrane integral enzymes thought to share a common membrane topology (Dyer & Mullen, 2001). This topology is characterized by at least four transmembrane helices, with loop regions with two or three histidine-containing 'His-boxes' coordinating iron atoms (Shanklin et al., 1994) involved in cytochrome-dependent catalysis at the cytosolic face of the ER, or ferredoxin-dependent at the stroma-face in the case of plastidial desaturases (Meesapyodsuk et al., 2007; Shanklin & Cahoon, 1998).

Studies on plant fatty acid desaturation have been motivated to some extent by an interest in seed oil modification and were focused on the biochemical or physiological analysis of lipid (oil)-associated fatty acid patterns (Browse et al., 1993; Cahoon et al., 1997; Heilmann et al., 2004; Lemieux et al., 1990; Miquel & Browse, 1992; Pidkowich et al., 2007). The desaturases FAD2 and FAD3 interact physically, enabling efficient substrate channeling from $18:1^{\Delta9}$ to $18:3^{\Delta9,12,15}$ with only limited release of the intermediate $18:2^{\Delta9,12}$ at the ER (Lou et al., 2014). By contrast, other membranes notably lack the capability to desaturate membrane lipids, necessitating the distribution of unsaturated lipids from their site of modification at the ER or in the plastid, respectively. This is also the case for non-oleogenic tissues, such as leaves, where especially FAD2 is a key element mediating membrane lipid desaturation outside the plastids (Okuley et al., 1994). In the vegetative part of the plant, the role of FAD2 in membrane homeostasis is thought to also contribute to plant stress tolerance (Lee et al., 2020; Nguyen et al., 2019; Zhang et al., 2012). In consequence, Arabidopsis *fad2* mutants display reduced tolerance to environmental stresses, such as high salt concentrations or during the ER stress response (Zhang et al., 2012).

Subcellular targeting has previously been found to be a key factor enabling the efficient interplay of fatty acid-modifying enzymes introduced in transgenic plants for optimal performance in biotechnology applications (Dyer & Mullen, 2001; Heilmann et al., 2012). However, analyzing the subcellular localization of such enzymes has not received much attention, and previous studies on plant FADs did not regularly include cell biological analyses. This is true even for key enzymes, such as FAD2 or the interacting FAD3, which are thought to reside at the ER mostly because they desaturate fatty acids associated with PC, a lipid prominent in the ER membrane. The mode of membrane insertion of FAD2 and FAD3 was previously analyzed based on biochemical studies on recombinant enzymes obtained by *in vitro* translation (McCartney et al., 2004). While these difficult studies confirmed ER residence and characterized sequence motifs mediating ER retention, their spatial resolution was intrinsically limited by the experimental approach. Importantly, McCartney

et al. (2004) speculated that both FAD2 or FAD3 might also be associated with the Golgi and almost 20 years ago proposed to resolve this question by biological imaging. Association of a functional EYFP-FAD2 fusion with the ER was subsequently reported based on confocal imaging in the context of a study on the ER stress response (Nguyen et al., 2019), but even though ER-untypical punctate structures were shown, the subcellular distribution was not analyzed in detail. Thus, despite the fundamental importance of FADs for plant physiology and biotechnology, precise information on the subcellular distribution of these enzymes has been scarce, even for an otherwise well-known enzyme, such as Arabidopsis FAD2. Analyzing the localization of FADs is technically not trivial, because the topology of these membrane integral enzymes must be considered. A main caveat is that fluorescence tags must not interfere with the formation of the catalytic center, nor with the N-terminal signal peptide or the C-terminal retention sequence, and therefore the physiological functionality of any fluorescent fusions must be carefully assessed.

Here, we analyze the subcellular localization of fluorescent FAD2-fusions at high resolution in intact Arabidopsis plants and in protoplasts, based on confocal *in vivo* imaging and quantitative image analysis. The fusion constructs used are first characterized for functionality in yeast and by Arabidopsis mutant complementation. Distribution patterns of the functional fusions are then tested against a range of coexpressed organellar fluorescence markers. The patterns indicate that FAD2 can associate with ER subdomains in close proximity to Golgi particles and are consistent with a role for FAD2 in contributing to the control of membrane unsaturation in cellular membranes, linked by the secretory pathway. The unusual C-terminal retention sequence of FAD2 is required for targeting the enzyme to these precise ER subdomains, and deletion or substitutions in this sequence result in a relaxed distribution pattern.

RESULTS

Fluorescence-tagged FAD2-fusions are functional in yeast

Fluorescent FAD2-fusions were first tested for functionality by heterologous expression in yeast and subsequent fatty acid analysis. To avoid masking of the C-terminal ER-retention motif (McCartney et al., 2004), the fluorescence proteins EYFP or mCherry were fused to the N-terminus of FAD2 (Figure 1A). Tagged or untagged FAD2 variants were expressed side-by-side in the yeast strain INVSc1 (Figure 1B,C), and cells harboring a vector with an empty expression cassette were used as negative control. Cultures were harvested and total fatty acid methyl esters (FAMEs) were analyzed by gas chromatography with flame ionization detection (GC-FID). Representative chromatograms and the quantification of individual FAMEs are shown in Figure 1(B). Chromatograms for FAD2,

(A)

(B)

(C)
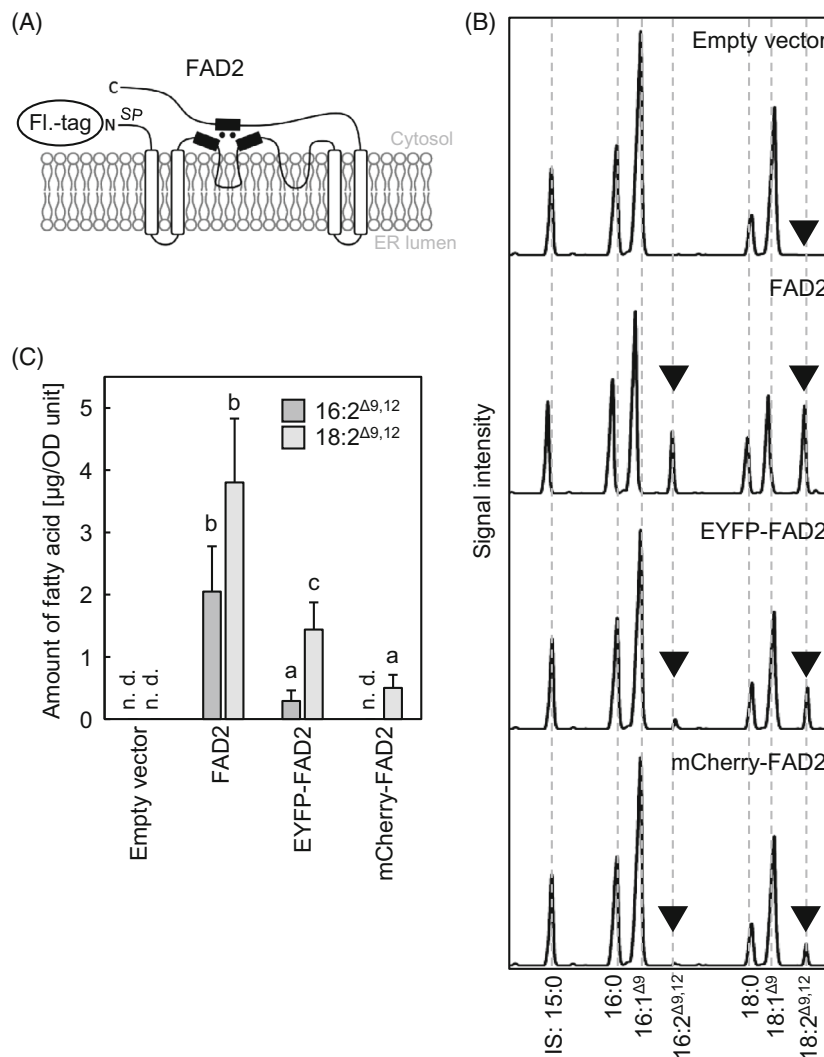
Figure 1. Fluorescence-tagged FAD2-fusions are functional in yeast.

The functionality of fluorescence-tagged variants of Arabidopsis FAD2 was assessed upon heterologous expression in the yeast *Saccharomyces cerevisiae*. Fusion proteins were expressed for 3 days at 20°C in the yeast strain INVSc1 in liquid SD-minimal medium without tryptophane containing 2% (w/v) galactose. The fatty acids from 20 OD-units were extracted, transmethylated, and analyzed by gas chromatography with flame ionization detection.

(A) Schematic representation of FAD2 with the position of the N-terminal fluorescence tag (FL.-tag). SP, signal peptide.

(B) Representative chromatograms of yeast expressing FAD2-variants. Arrowheads indicate the signals for $16:2^{\Delta9,12}$ and $18:2^{\Delta9,12}$, the products of FAD2-mediated conversion of endogenous oleic acid.

(C) The amounts of $16:2^{\Delta9,12}$ and $18:2^{\Delta9,12}$ from four independent experiments with two biological replicates each were quantified and are presented in the bar chart. Data represent mean $\pm$ standard deviation from four independent experiments. Letters indicate categories of significant differences determined by one-way ANOVA with a Tukey's *post-hoc* test ($P < 0.05$). IS, internal standard (tripentadecanoin); n.d., not detectable.

EYFP-FAD2, or mCherry-FAD2 contained additional fatty acid peaks for linoleic acid ($18:2^{\Delta9,12}$), the product of FAD2-mediated conversion of oleic acid, which was not present in the control cells yeast harboring an empty vector (Figure 1B). Yeast transformed with the untagged FAD2 contained the most $18:2^{\Delta9,12}$ and $16:2^{\Delta9,12}$, a byproduct of FAD2-mediated desaturation based on conversion of $16:1^{\Delta9}$ (Figure 1B,C). Besides $18:2^{\Delta9,12}$, $16:2^{\Delta9,12}$ was also detectable in yeast expressing EYFP-FAD2 but not in cells expressing mCherry-FAD2 (Figure 1B, as indicated). The formation of $18:2^{\Delta9,12}$ (Figure 1C) indicates that the

N-terminal EYFP-FAD2, as well as mCherry-FAD2 fusions, were functional as oleoyl $\Delta12$-desaturases in yeast.

Fluorescence-tagged FAD2 fusions complement and restore linoleic acid biosynthesis in the Arabidopsis *fad2-1* mutant

EYFP-FAD2 was next tested for *in planta*-functionality in the Arabidopsis *fad2-1* background, driven by an intrinsic promoter fragment consisting of 2281 bp of genomic sequence upstream of the start codon of the *FAD2* coding sequence (*pFAD2*). Plants were transformed by

Agrobacterium tumefaciens infection and floral dipping (Clough & Bent, [1998]), and three resistant lines, L1, L2, and L3, were chosen for further experiments (termed EYFP-FAD2 plants). While the Arabidopsis *fad2-1* mutant has reduced levels of linoleic acid, it does not display a macroscopic growth defect under standard growing conditions. Transgene expression did not impair growth, as evident from wild type controls, *fad2-1* mutants, and EYFP-FAD2 plants grown side-by-side on soil (Figure 2A). When fatty acids were extracted from seeds, transmethylated, and analyzed by GC-FID, the expression of EYFP-FAD2 in the *fad2-1* mutant background restored the ability to form $18:2^{\Delta9,12}$ (Figure 2B,C). While the relative amount of $18:2^{\Delta9,12}$ in the *fad2-1* mutant was reduced to ~5% of the total fatty acids, compared to ~25–30% of the total fatty acids in wild type, the EYFP-FAD2 lines L1–L3 contained ~15–25% of $18:2^{\Delta9,12}$ in seeds, representing a significant increase over the levels of the *fad2-1* mutant (Figure 2B). Moreover, the characteristic accumulation of the metabolic precursor $18:1^{\Delta9}$ in the *fad2-1* mutant was not present in wild type controls or the EYFP-FAD2 complemented lines (Figure 2C), and the complemented plants had a similar seed fatty acid composition as the wild type controls.

In addition to the analysis of seed fatty acids, the fatty acid composition was also examined in PC, MGDG and DGDG isolated from 14-day-old seedlings (Figure 3). The relative amounts of lipid-associated $18:2^{\Delta9,12}$ indicate a reduction of PC-bound $18:2^{\Delta9,12}$ to below 5% of the total fatty acids in the *fad2-1* mutant, compared to more than 35% of the total fatty acids in wild type (Figure 3A, left panel). The amounts of PC-associated $18:2^{\Delta9,12}$ in the complemented EYFP-FAD2 lines L1–L3 were not significantly different from values for the wild type, with the exception of line EYFP-FAD2 L2 still showing a minor reduction (Figure 3A, left panel). Furthermore, the analysis of fatty acids associated with PC (Figure 3A, right panel) showed an increased proportion of $18:1^{\Delta9}$ for the *fad2-1* mutant, concomitant with a reduction in $18:2^{\Delta9,12}$ and $18:3^{\Delta9,12,15}$. By contrast, in the EYFP-FAD2 lines L1–L3, $18:2^{\Delta9,12}$ constituted around 30% of PC-associated fatty acids and thus significantly more than in the *fad2-1* mutant, indicating successful complementation. Effects of the *fad2-1* mutation were restricted largely to PC, and the amounts of $18:2^{\Delta9,12}$ or other fatty acids associated with the plastidial glycolipids, MGDG or DGDG (Figure 3B,C, right panels, respectively), did not substantially differ between the wild type controls, the *fad2-1* mutant or the EYFP-FAD2 expressing lines, with only a slight increase of DGDG-associated $18:1^{\Delta9}$ observed in the *fad2-1* mutant (Figure 3C, right panel). The data show that the expressed EYFP-FAD2 fusion was functional *in planta* and specifically modified fatty acids associated with the extraplastidial membrane lipid, PC.

The *in planta* functionality of the EYFP-FAD2 fusion was further tested by assessing salt sensitivity, as the *fad2-1* mutant displays reduced tolerance to salt (Zhang et al., [2012]) (Figure S1). Two-week-old seedlings of wild type controls, *fad2-1* mutants or the transgenic lines L1–L3 were grown on media containing 0, 75, 100 or 125 mM of NaCl, and the root length of the seedlings was recorded (Figure S1A). In all regimes tested, the *fad2-1* mutant displayed a significant reduction in root length compared to wild type controls, whereas the lines L1–L3 displayed wild type-like root growth (Figure S1B).

Overall, the expression of EYFP-FAD2 complemented both macroscopic and biochemical phenotypes of the *fad2-1* mutant, indicating the EYFP-FAD2 fusion was functional *in planta*, so its subcellular distribution could next be assessed in a meaningful context.

EYFP-FAD2 fusions decorate small, donut-shaped cytoplasmic structures

The subcellular distribution of fluorescent FAD2 fusions was analyzed in roots and leaves of 7-day-old *fad2-1* Arabidopsis seedlings expressing EYFP- or mCherry-FAD2 under the control of the intrinsic promoter fragment. To analyze the localization pattern in the seedlings under minimal stress by laser illumination, the subcellular distribution of EYFP-FAD2 was first examined by light sheet microscopy using a Zeiss Lightsheet Z1 microscope and then in more detail by laser scanning confocal microscopy (LSM) using a Zeiss LSM880 Airyscan FAST system (LSM). Figure 4 shows the localization pattern of EYFP-FAD2 in roots (Figure 4A,B) or in leaf epidermal cells (Figure 4C,D). Overview images by light sheet microscopy indicated EYFP-FAD2 in a pattern of mobile cytoplasmic dots (Figure 4A). When analyzed at higher resolution by LSM, the EYFP-FAD2 marker decorated small and mobile donut-shaped structures in the cytoplasm (Figure 4B–D). Coexpression of mCherry-FAD2 (mC-FAD2) with the ER marker GFP-HDEL in leaves highlights the difference in the distribution of the donut-shaped puncta versus a network-like distribution of the ER marker (Figure 4D). Importantly, the synchronous imaging of the donut-shaped mC-FAD2 pattern and the ER marker indicates that the mC-FAD2 distribution did not reflect an unusual appearance of the ER, for instance as fusiform bodies induced by stress or during certain developmental stages (e.g., Yamada et al., [2011]). Instead, the particulate distribution of mC-FAD2 appeared together with a network-like distribution of the GFP-HDEL marker (Figure 4D). This experiment also illustrates that the fluorophore did not influence the localization of the FAD-fusions, as both EYFP-FAD2 and mC-FAD2 displayed equivalent patterns (for comparison, Figure 4B–D). The observation of EYFP-FAD2 decorating cytoplasmic hollow-shaped particulate structures, rather than displaying a diffuse and
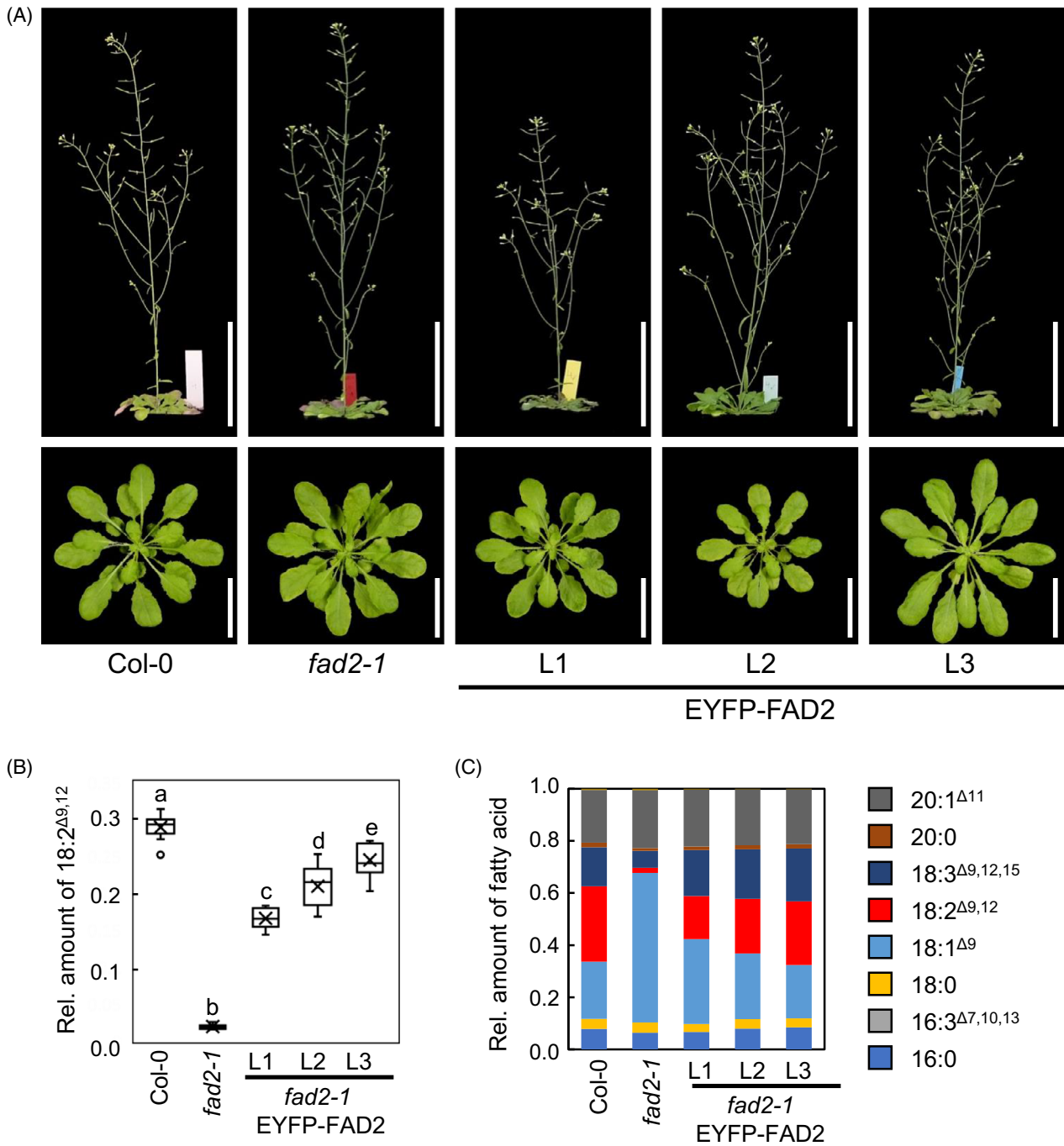
Figure 2. Ectopic expression of EYFP-FAD2 restores linoleic acid biosynthesis in the Arabidopsis *fad2-1* mutant.

EYFP-FAD2 was expressed in the Arabidopsis *fad2-1* mutant background under the control of an endogenous promoter fragment and three independent T2 lines (L1–L3) were analyzed for phenotypic and biochemical complementation. Wild type and the *fad2-1* mutant served as controls.

(A) Phenotypic appearance of 12-week-old (upper panels) and 8-week-old (lower panels) plants. All plants were grown under short-day conditions (8 h light, 16 h dark) for 8 weeks. Twelve-week-old plants were grown for four additional weeks under long-day conditions (16 h light, 8 h dark). Images are representative of 11 plants analyzed for each genotype.

(B) The relative amount of $18:2^{\Delta9,12}$ in seeds was analyzed. Significant differences were determined using one-way ANOVA with a Tukey's *post-hoc* test ($P < 0.05$). Different letters indicate significantly different categories of samples.

(C) The global fatty acid composition of seeds was analyzed in *fad2-1* mutants ectopically expressing EYFP-FAD2 under the control of its intrinsic promoter. Data are representative of 10 plants analyzed per line.

18:2$^{\Delta9,12}$ associated with

Fatty acids associated with
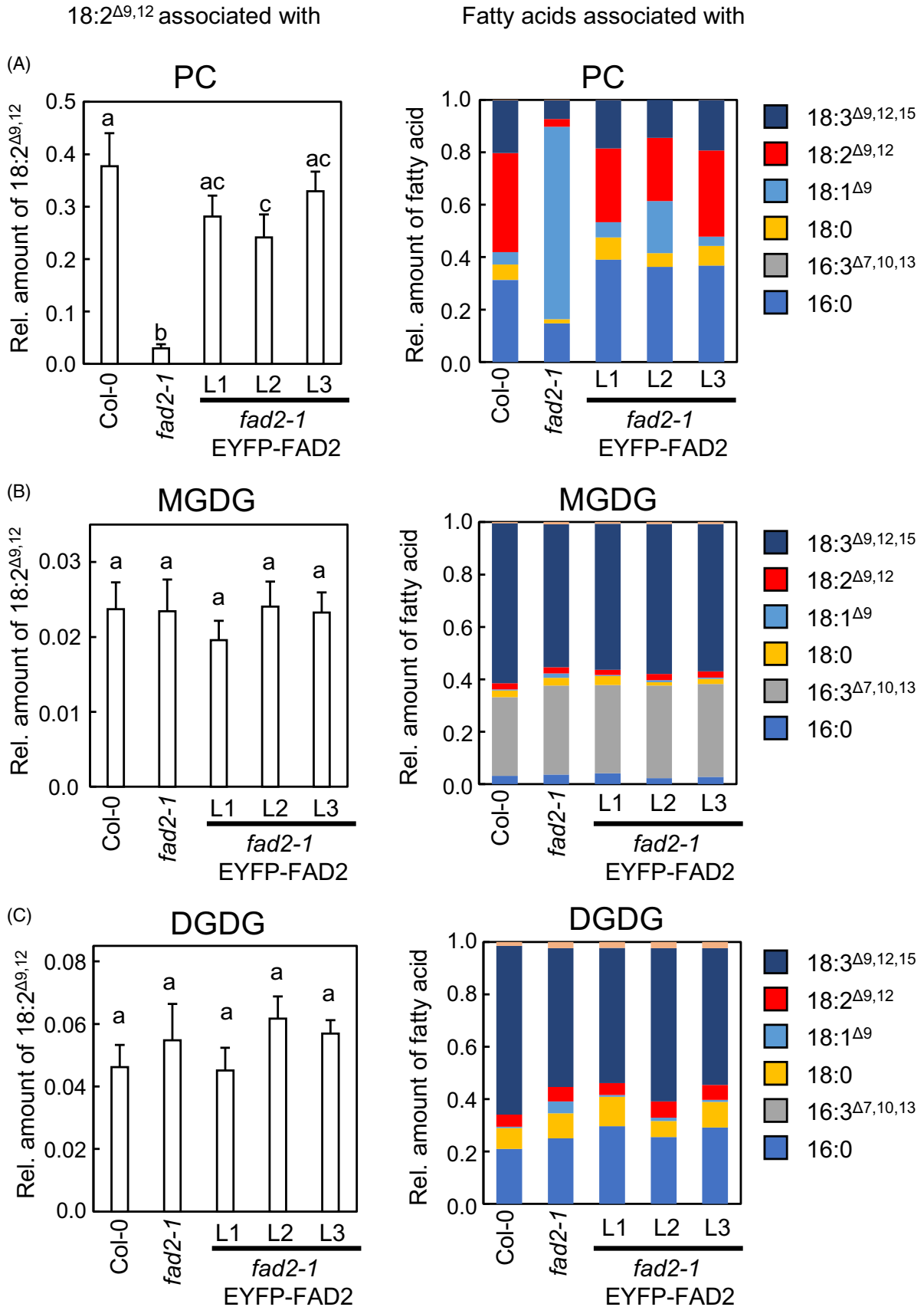
Figure 3. Linoleic acid formed by EYFP-FAD2 is associated with phosphatidylcholine.
The relative amounts of $18:2^{\Delta9,12}$ and the global fatty acid composition were analyzed for different lipid classes isolated from seedlings of three independent T2 lines (L1–L3) expressing EYFP-FAD2 under the control of an endogenous promoter fragment in the *fad2-1* mutant background. Wild type and the *fad2-1* mutant served as controls. Seedlings were grown for 14 days on ½ MS medium under long-day conditions (16 h light, 8 h dark).
(A–C) The relative amounts of $18:2^{\Delta9,12}$ (left panels) and the global fatty acid composition associated with PC (A), MGDG (B), and DGDG (C), as indicated. Data on the relative amounts (left panels) represent mean ± standard deviation from three independent experiments. Significant differences were determined using one-way ANOVA with a Tukey's *post-hoc* test ($P < 0.05$). Different letters indicate significantly different categories of samples. Data for the global fatty acid analyses (right) are from the same data set and are representative of three independent experiments.

network-like ER pattern, was unexpected in light of previously published work describing ER association of FAD2 (McCartney et al., 2004; Nguyen et al., 2019).

Fluorescent fusions of FAD2 associated with cytoplasmic donut-shaped structures in Arabidopsis mesophyll protoplasts

As the successful mutant complementation (Figures 2 and 3) indicated functionality of the fluorescent FAD2-fusions, and therefore biological relevance of the fluorescence distributions observed, it was next attempted to identify the nature of the particulate structures decorated by EYFP-FAD2 in Arabidopsis mesophyll protoplasts. The protoplast system combines the advantages of fast and easy usage of different organelle markers for coexpression experiments with the possibility of live cell imaging in the homologous organism (Arabidopsis). Mesophyll protoplasts were isolated from Arabidopsis wild type or an ER-marker line expressing GFP-HDEL and (co-)transformed with expression vectors for fluorescence-tagged FAD2 as well as with other organelle markers. Fluorescence distributions were analyzed by LSM, or by spinning disc (SD) microscopy. Images were acquired as z-stacks covering the cell from one edge to the center and individual frames or maximum-intensity projections were used for image analyses. The subcellular distribution of an EYFP-FAD2 fusion was analyzed first without the potential interference of any additional organelle markers (Figure 5). In mesophyll protoplasts, EYFP-FAD2 localized to small mobile circular structures (Figure 5A,B). Higher magnification clearly shows a lower fluorescence intensity in the center of the circular structures decorated by EYFP-FAD2, compared to the periphery (Figure 5B,C). Importantly, the fluorescence distribution of EYFP-FAD2 in Arabidopsis protoplasts was similar to that observed in stably transformed plant lines (cf. Figure 4). To rule out an effect of the EYFP fluorophore on the subcellular distribution of the EYFP-FAD2 fusion in protoplasts, the distribution of mC-FAD2 fusion was also analyzed (Figure 5D), and the mC-FAD2 marker decorated donut-shaped particulate structures in a pattern comparable to that of EYFP-FAD2, indicating that the nature of the fluorophore did not influence the localization of the fluorescent FAD2 fusions to the small circular structures. To assess the integrity of fluorescent fusions of FAD2, immunodetection of mC-FAD2 expressed in protoplasts shown

in Figure 5(D) was performed. Immunodetection using an antiserum against mCherry indicates mC-FAD2 fusion proteins of the correct size of 71 kDa with little or no degradation, confirming the integrity of the fluorescent fusions (Figure S2).

Fluorescent fusions of FAD2 closely associate with Golgi particles

To assess the identity of the small and mobile circular structures decorated by fluorescent fusions of FAD2, coexpression experiments with organelle markers were performed in Arabidopsis protoplasts, and confocal z-stacks were recorded by LSM. To quantify the degree of colocalization with the individual markers, Pearson's correlation coefficients (PCC) were calculated based on the z-stacks using the Fiji plugin JACoP (Bolte & Cordelieres, 2006). PCC analyze the linear relation of two fluorescence images and can range from −1 to 1 (with −1 reflecting perfect, linear, inverse relation and 1 indicating perfect, linear positive correlation of the fluorescence intensities of two channels). To assess the technical resolution of this approach in our experimental system, ER or Golgi markers were coexpressed in mesophyll protoplasts in different combinations, and the respective PCCs were determined (Figure S3). The combinations of markers tested included ER markers, consisting of either mCherry or EYFP fused between the N-terminal signal peptide of the wall-associated kinase 2 (AtWAK2) and the C-terminal ER-retention signal sequence HDEL (ER-mC or ER-EYFP) (Stellmach et al., 2022); ER-mC versus a *cis*-Golgi marker representing the first 49 amino acids of α-1,2-mannosidase I from *Glycine max* (Nelson et al., 2007; Saint-Jore-Dupas et al., 2006), fused to a C-terminal EYFP-tag (Man1-EYFP); pre-*cis*-Golgi markers consisting of the full-length ER-α-mannosidase I from *Arabidopsis thaliana* (Schoberer et al., 2019) fused to C-terminal fluorescence tags (MNS3-mC or MNS3-EYFP); or the *cis*-Golgi marker Man1-mC versus a *trans*-Golgi marker consisting of the first 76 amino acids of α-2,6-sialyltransferase from *Rattus norvegicus* (Wee et al., 1998), fused to a C-terminal fluorescence-tag (ST-EYFP). Based on the imaging conditions determined in these control experiments (Figure S3), the respective distribution patterns of fluorescent FAD2-variants were assessed.

FAD2 is thought to contain a C-terminal ER retention signal targeting the enzyme to the ER of Arabidopsis root

cells (Dyer & Mullen, 2001; McCartney et al., 2004; Nguyen et al., 2019). Therefore, association of EYFP-FAD2 with the ER was tested first, even though the donut-shaped distribution pattern observed in leaves and mesophyll protoplasts did not resemble typical ER-association (cf. Figure 4). EYFP-FAD2 was expressed under its endogenous
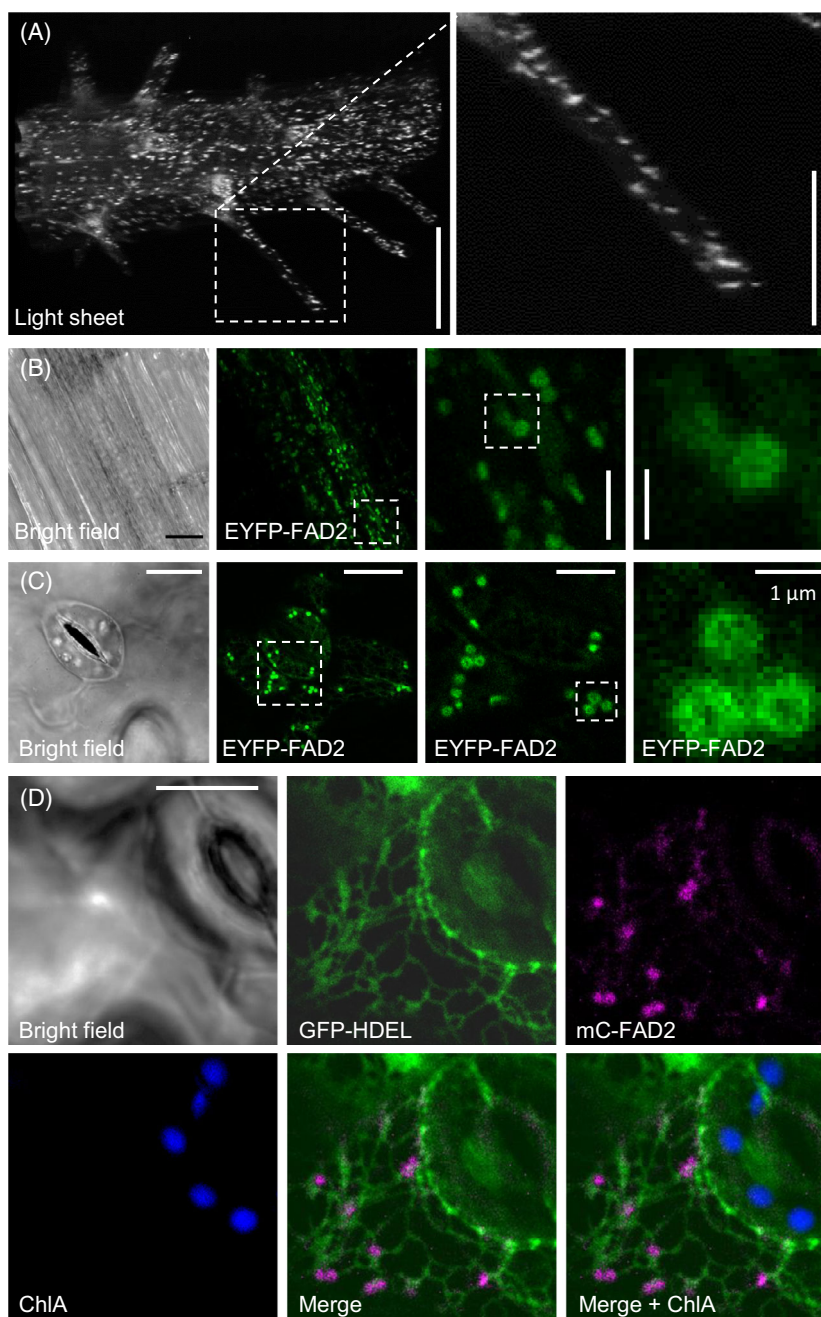
Figure 4. Functional fluorescent FAD2 fusions decorate small, donut-shaped cytoplasmic structures in roots and leaves of Arabidopsis.

Seven-day-old seedlings of Arabidopsis lines expressing the functional EYFP-FAD2 marker under its intrinsic promoter were grown on ½ MS medium under long-day-conditions (16 h light, 8 h dark) and the fluorescence distribution was analyzed by light sheet microscopy in roots (a) or by LSM in roots or leaves (B–D).

(A) Light sheet microscopy of elongating root cells and root hairs. Right panel, magnification of dashed box area. Scale, 40 μm (left); 20 μm (right).

(B) Fluorescence distribution of EYFP-FAD2 in elongating root cells. Dashed boxes, areas selected for magnification in the right-hand panels. Scale, 10 μm (left), 5 μm (center), 1 μm (right).

(C) Fluorescence distribution of EYFP-FAD2 in epidermal pavement cells. Dashed boxes, areas selected for magnification in the right-hand panels. Scale, 10 μm (left), 5 μm (center), 1 μm (right).

(D) Distribution of mCherry-FAD2 (mC-FAD2) in leaf epidermal cells coexpressing the ER marker, GFP-HDEL. Chlorophyll *A* (ChlA) autofluorescence is depicted in blue. Scale, 15 μm. Images are representative 2 (A), 14 B), 14 C), and 5 (D) experiments using plants representing three independent transgenic lines. [Correction added on 14 October 2023, after first online publication: The part labels for Figures 4, 5 and 7 have been changed to upper case in this version.]
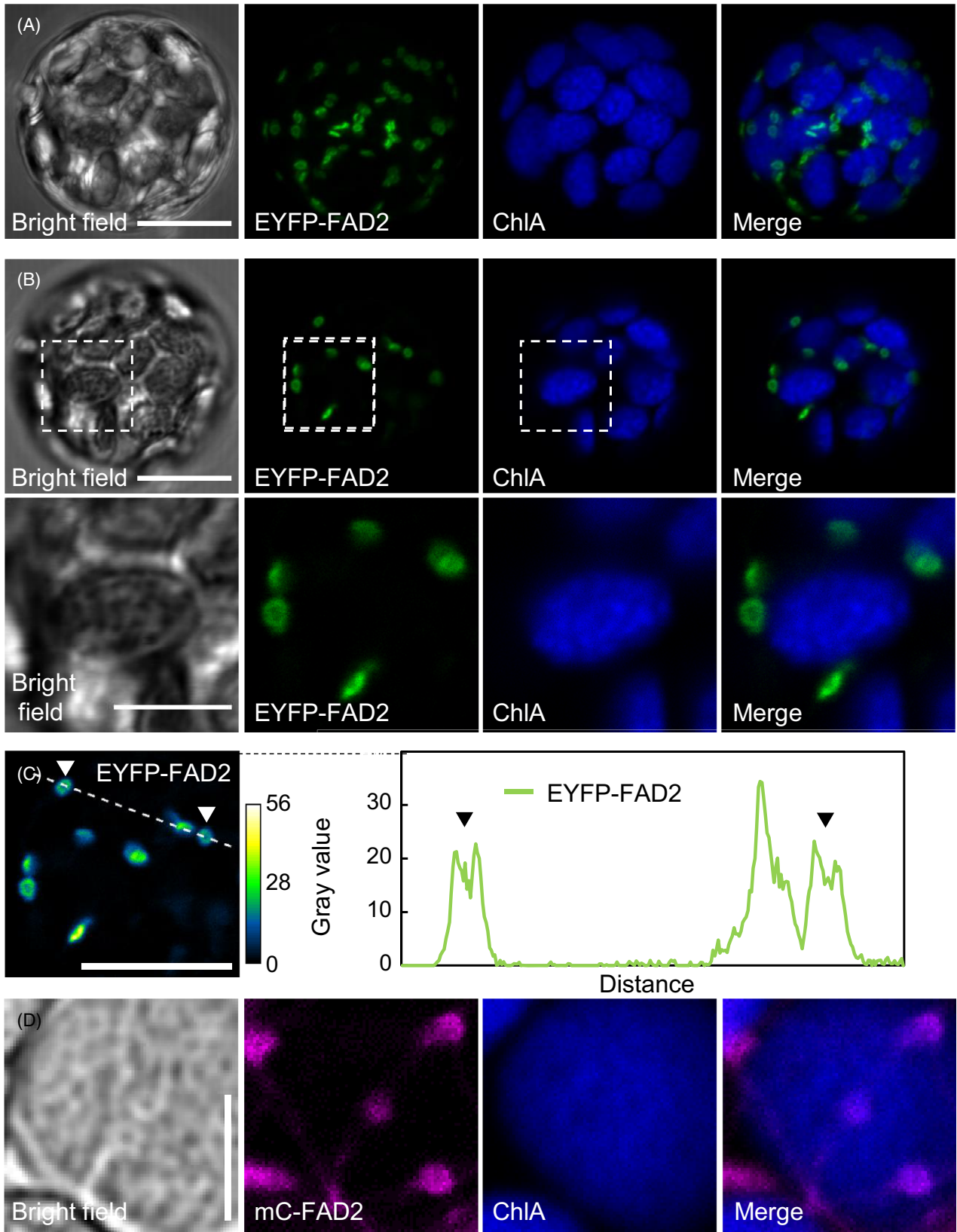
promoter in Arabidopsis protoplasts together with the ER-marker ER-mC. Representative z-stack images and the PCCs for the co-localization are shown in Figure 6(A–D). While EYFP-FAD2 was again seen in small mobile circular structures, the ER-marker formed a diffuse network throughout the cytosol, as is typical for ER (Figure 6A,B). EYFP-FAD2 intensity coincided with ER-mC in detailed line-intensity profiles (Figure 6C), suggesting that even though EYFP-FAD2 was not evenly distributed throughout the ER, the punctate structures marked by EYFP-FAD2 nonetheless were all associated with the broader ER network. The PCC for EYFP-FAD2 against mC-HDEL ranged between 0.4 and 0.8, with a mean of 0.6 (Figure 6D). Overall, the subcellular distribution of EYFP-FAD2 and the ER marker did not fully coincide, and consequently, the average PCC was lower than that observed for the two ER markers (see Figure S3). Next, based on the appearance of the localization pattern of EYFP-FAD2 in stably transformed plants (cf. Figure 4C,D), the distribution was tested relative to the coexpressed *cis*-Golgi-marker, Man1-mC (Figure 6E–H). Arabidopsis protoplasts were cotransformed with EYFP-FAD2 and Man1-mC and analyzed by LSM or SD (Figure 6E–G). EYFP-FAD2 and Man1-mC localized to overlapping circular structures or appeared as short lines (Figure 6E,F). A line plot analyzed from a single confocal section illustrates a high concurrence of EYFP-FAD2 and Man1-mC fluorescence (Figure 6G). PCCs calculated for z-stacks acquired by LSM ranged from 0.5 to 0.8, with a mean of 0.66 for the correlation of EYFP-FAD2 and Man1-mC (Figure 6H), with significantly lower PCCs against chlorophyll A. The PCC for the co-localization of EYFP-FAD2 and Man1-mC was slightly higher than for the co-localization with the ER marker and less scattered (see Figure 6H) but were still lower than the value of ~0.9 observed for example, for co-localization of two MNS3-markers (cf. Figure S3). While side-by-side assessment of fluorescence distribution patterns for EYFP-FAD2 and Man1-mC showed an intuitive similarity (Figure 6E–G), the rather low PCCs for coexpressed EYFP-FAD2 and *cis*-Golgi-mC were likely a consequence of the high mobility of the particulate structures during live imaging. High-resolution imaging was used to determine the distribution patterns also in relation to the *trans*-Golgi marker, ST-mC (Figure 6I,J). The relative distribution of EYFP-FAD2 and *cis*-Golgi-mC or *trans*-Golgi-mC, respectively, was analyzed by LSM in Airyscan FAST mode, providing high spatial and temporal resolution (Figure 6I). The EYFP-FAD2 marker again colocalized substantially with Man1-mC, as indicated by the white overlap in merged images (Figure 6I) and by a high PCC (Figure 6J), whereas the overlap of EYFP-FAD2 with ST-mC was significantly lower (Figure 6I,J). While the high mobility of the EYFP-FAD2 signals poses a challenge to imaging at this resolution, we conclude that EYFP-FAD2 might be associated with *cis*-Golgi rather than *trans*-Golgi

cisternae. Circular structures marked by EYFP-FAD2 might represent face-on views of Golgi-stacks, whereas an appearance as short lines suggests a flattened disc shape when imaged from the side, as previously described for Golgi (Nebenfuhr et al., 1999).

Detailed localization analysis indicates EYFP-FAD2 at pre-*cis*-Golgi stacks at ER exit sites

As the localization of EYFP-FAD2 did not fully coincide with the Man1-mC marker, the association of EYFP-FAD2 with Golgi particles was analyzed in further detail. During the imaging of EYFP-FAD2 in protoplasts and leaf epidermal cells, EYFP-FAD2 fluorescence was often visible as hollow donut-like shapes, whereas this hollow shape was not observed for the Man1-mC marker. This difference was confirmed by line plots derived from images recorded by SD imaging for fast acquisition of the highly mobile signals (Figure 7A). The dimensions of the EYFP-FAD2-marked structures and Golgi-mCherry marked structures coincided well when images were rapidly acquired by SD, both in face-on views and in side views, respectively (Figure 7A, Detail image), and the fluorescence intensity of Man1-mC (red) reached a maximum in the middle of the Golgi-stacks in face-on views, whereas EYFP-FAD2 fluorescence (green) slightly decreased in the center of the area decorated by the marker compared to the periphery. A reduction in fluorescence intensity of EYFP-FAD2 but not Man1-mC at the center of the rings is evident from two-channel line intensity plots (Figure 7A, lower left panel). Further experiments included the analysis of EYFP-FAD2 relative to an MNS3-mC pre-*cis*-Golgi marker (Figure 7B). While EYFP-FAD2 and MNS3-mC were distributed in very similar patterns both in face-on views and in side-views, MNS3-EYFP did not decorate donut-shaped structures but was rather located within donuts decorated by EYFP-FAD2 (Figure 7B). By contrast, another pre-*cis*-Golgi marker, consisting of full-length Golgin-84A from *A. thaliana* (Vieira et al., 2020) fused to an N-terminal mCherry tag (mC-Golgin-84A) decorated donut-shaped structures that largely overlapped with structures labeled by EYFP-FAD2 (Figure 7C). The colocalization was obvious also from the mixed red/green fluorescence pattern on the surface of the fluorescent particles observed (see detail face-on view in Figure 7C). As the ring-shaped structures decorated by mC-Golgin-84A appeared somewhat larger than those decorated by EYFP-FAD2 (Figure 7C), we estimate the position of EYFP-FAD2 to be between those of MNS3-mC and mC-Golgin-84A at pre-*cis*-Golgi cisternae. To further elucidate the localization of EYFP-FAD2 at pre-*cis*-Golgi-stacks, it was next analyzed how EYFP-FAD2-marked particles distributed relative to an ER-marker. Representative images of coexpressed EYFP-FAD2 and ER-mC are shown in Figure 7(D). The Fiji-plugin 'Colocalization' (https://imagej.nih.gov/ij/plugins/colocalization.html) marks co-localizing pixels fulfilling set

The Plant Journal published by Society for Experimental Biology and John Wiley & Sons Ltd.,
The Plant Journal, (2024), **117**, 242–263

Figure 5. Fluorescent fusions of FAD2 associated with cytoplasmic donut-shaped structures in Arabidopsis mesophyll protoplasts.

Arabidopsis mesophyll protoplasts were transiently transformed with *pEntryA-pFAD2::EYFP-FAD2* and analyzed by LSM. z-Stacks of 20–30 optical sections were generated with ~0.6 μm distance. EYFP-FAD2 fluorescence is depicted in green, and the autofluorescence of chlorophyll A (ChlA) is shown in blue. Scale, 10 μm.

(A) Maximum intensity projection of a z-stack. Scale, 10 μm.

(B) Median confocal section of the z-stack from (A). Lower panels, magnification of the dashed box area. Scale, 10 μm (upper), 5 μm (lower).

(C) Intensity profile for EYFP-FAD2 along the line highlighted in the left panel [median confocal section from (B)]. Arrowheads indicate the lower fluorescence intensity in the center of the rings.

(D) Arabidopsis mesophyll protoplasts were transiently transformed with *pEntryA-pFAD2::mCherry-FAD2* and analyzed by LSM. Blue, chlorophyll A (ChlA) auto-fluorescence. Scale, 5 μm. Images and analyses are representative of cells analyzed in 14 (A–C) or 3 (D) independent transformation experiments.

---

thresholds as white pixels, allowing easy visual evaluation of co-localization. The computer-aided co-localization analysis (Figure 7D) shows the white co-localizing pixels encircling each EYFP-FAD2-marked signal, indicating that EYFP-FAD2 overlapped with the ER-mC marker at pre-*cis*-Golgi-stacks decorated by EYFP-FAD2 fluorescence (cf. Figure 7A). In 24 analyzed z-stack images representing >250 signals analyzed, no EYFP-FAD2 signal was observed independently of the ER-mC marker. Together, these analyses identify the position of the EYFP-FAD2 marker at pre-*cis*-Golgi cisternae around ER-Golgi-exit sites.

Fluorescent fusions of FAD2 do not coincide with fluorescent markers for oil bodies or peroxisomes

While EYFP-FAD2 distribution positively correlated with *cis*-Golgi-mC signals, further analyses were performed to rule out coincidental correlations, and EYFP-FAD2 was coexpressed with peroxisome- and oil-body-markers, two other mobile and mainly circular cell organelles related to lipid metabolism. The relative distribution of EYFP-FAD2 and peroxisomes was assessed using peroxisome-targeted CFP (CFP-SKL; Figure S4A–C). CFP-SKL marked circular structures of a similar size as EYFP-FAD2, but the fluorescence signals did not co-localize. The PCCs for the correlation of EYFP-FAD2 and CFP-SKL ranged from 0.25 to 0.67, with a mean of 0.46 and were not different from values obtained for EYFP-FAD2 versus chlorophyll A (Figure S4B), indicating that EYFP-FAD2 did not co-localize with CFP-SKL. The line plot presented in Figure S4(C) also illustrates the incongruent fluorescence distribution of EYFP-FAD2 and CFP-SKL. As an oil body marker, Oleosin3 (OLE3) fused to mCherry was used (Figure S4D–F). Similar to coexpression of EYFP-FAD2 and CFP-SKL, OLE3-mCherry (OLE3-mC, magenta) and EYFP-FAD2 (green) both localized in circular structures of approximately similar size but without obvious co-localization. The structures marked by OLE3-mC varied more in size than EYFP-FAD2 signals (Figure S4D). The PCCs shown for EYFP-FAD2 versus OLE3-mC in Figure S4(E) ranged from 0.05 to 0.67, with a mean of 0.34 for the correlation of EYFP-FAD2 and OLE3-mC and were not different from both correlations to chlorophyll *A*. A line plot of EYFP-FAD2 and OLE3-mC fluorescence distribution (Figure S4F) illustrates that EYFP-FAD2 and OLE3-mC did not distribute in a coinciding pattern.

The C-terminal unusual retention sequence mediates precise localization of EYFP-FAD2

The data so far (Figures 4–7) indicated that in the tissues analyzed EYFP-FAD2 localized to an unexpectedly narrow ER sub-region at the ER-Golgi transition. As membranes form a dynamic continuum between ER and Golgi, the observed localization pattern of fluorescence-tagged FAD2 raised the question of how the enzyme maintained its precise subcellular position. Therefore, the contribution of the previously described unusual retention sequence at the C-terminus of FAD2 was analyzed in more detail (Figure 8). Both the deletion of the five C-terminal residues YNNKL (FAD2 ΔYNNKL) or the substitution of two large hydrophobic (Y/L) to small hydrophobic residues (A/A) within that sequence (FAD2 ANNKA) influenced the subcellular localization of the EYFP-FAD2 variants. Both EYFP-FAD2 ΔYNNKL (Figure 8B,C) or EYFP-FAD2 ANNKA (Figure 8D,E) lost the association with small mobile particles (Figure 8B, D, upper panels) and now displayed a relaxed localization pattern coinciding with an ER marker (Figure 8B,D, lower panels, Figure 8C,E, respectively). These observations indicate (i) that the C-terminal YNNKL motif is required for the precise positioning of EYFP-FAD2 at the ER-Golgi transition; and (ii) that ER-association of EYFP-FAD2 is mediated by another mechanism not involving the extreme C-terminus. To assess the biochemical functionality of EYFP-FAD2 ΔYNNKL and EYFP-FAD2 ANNKA, the FAD2 variants were heterologously expressed in yeast, total fatty acids were extracted and transmethylated, and the formation of linoleic acid and/or hexadecadienoic acid from endogenous fatty acid precursors was analyzed by GC-FID as before (Figure S5). Expression of EYFP-tagged wild type FAD2 (EYFP-FAD2) served as a positive control. While all EYFP-tagged fusions were detected in the yeast cells by fluorescence (Figure S5A), only the expression of the EYFP-FAD2 control yielded detectable amounts of linoleic acid and hexadecadienoic acid (Figure S5B), whereas neither fatty acid was detected upon expression of EYFP-FAD2 ΔYNNKL or EYFP FAD2 ANNKA (Figure S5B). The data suggest that the C-terminus of FAD2 is required for its functionality. Please note that EYFP-tagged FAD2 variants distributed in yeast cells in a pattern possibly representing ER (Figure S5A); however, unlike Arabidopsis, baker's yeast does not have organized Golgi stacks. As more
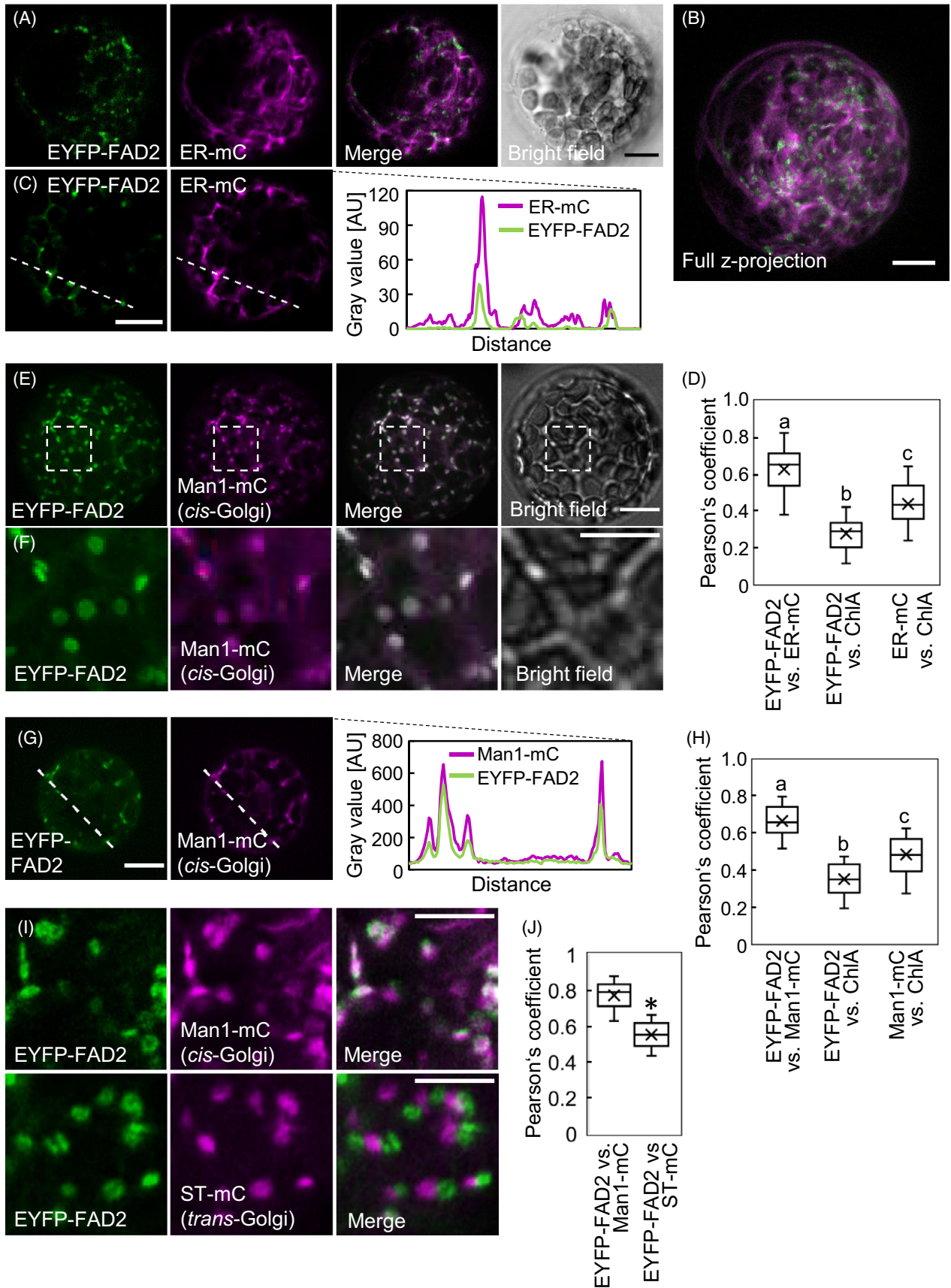
Figure 6. EYFP-FAD2 closely associates with Golgi particles in Arabidopsis mesophyll protoplasts.

The nature of the cytosolic particles decorated by EYFP-FAD2 was assessed relative to coexpressed markers for ER or Golgi. Arabidopsis mesophyll protoplasts were cotransformed with *pEntryA-pFAD2::EYFP-FAD2* and either the ER-marker construct *CD3-959-ER-mCherry* [ER-mC (A–D)] or with the Golgi-marker construct *CD3-967-Golgi-mCherry* [*cis*-Golgi-mC (D–F)] and analyzed by LSM or SD. z-Stacks of 20–30 slices were generated with ~0.6 µm distance. EYFP-FAD2 fluorescence is depicted in green, and the organelle markers in magenta. Scale, 10 µm.

(A) Median confocal section of a protoplast cotransformed with EYFP-FAD2 and ER-mC analyzed by LSM.

(B) Maximum intensity projection of the z-stack used for (A). Scale, 10 µm.

(C) Fluorescence intensity of EYFP-FAD2 and ER-mC along the dashed line, as indicated.

(D) PCCs for EYFP-FAD2 versus ER-mC calculated from 22 z-stacks acquired by LSM. Letters indicate significant differences ($p < 0.05$) according to a one-way ANOVA test with Tukey's post-hoc test.

(E–H) Coexpression of EYFP-FAD2 with *cis*-Golgi-mC, acquired by SD. (E) Median confocal section of a protoplast cotransformed with EYFP-FAD2 and *cis*-Golgi-mC. Scale, 10 µm.

(F) Magnification of the area marked by dashed boxes in (E). Scale, 5 µm.

(G) Fluorescence intensity of EYFP-FAD2 and *cis*-Golgi-mC along the dashed line, as indicated.

(H) PCCs for EYFP-FAD2 versus *cis*-Golgi-mC calculated from 14 z-stacks. Letters indicate significant differences ($P < 0.05$) according to a one-way ANOVA test with Tukey's post-hoc test.

(I) Coexpression of EYFP-FAD2 with *cis*-Golgi-mC (upper panels) or with *trans*-Golgi-mC (lower panels), acquired by LSM in Airyscan FAST mode. Scale, 5 µm.

(J) PCCs for EYFP-FAD2 versus ER-mC or for EYFP-FAD2 versus *trans*-Golgi-mC, as indicated, each calculated from 20 z-stacks acquired by LSM in Airyscan FAST mode. The asterisk indicates a significant difference according to a Student's t-test ($P < 0.05$).

subtle differences in localization are not easily interpreted in yeast cells, we choose to interpret the observed fluorescence (Figure S5A) only as an indication of positive expression of the fusion proteins.
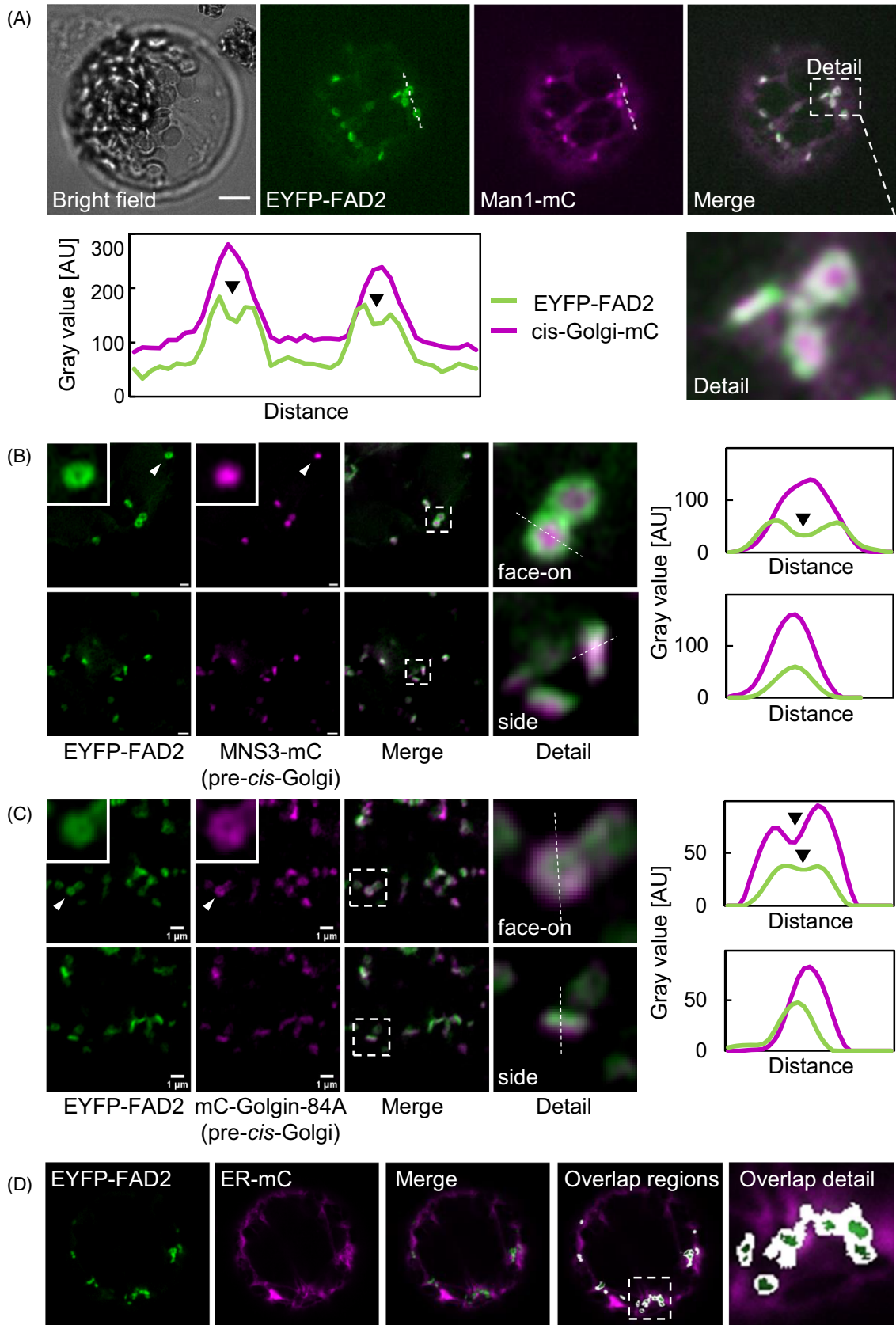
FAD2 at the ER-Golgi transition influences plasma membrane liquid phase order

The observed localization of EYFP-FAD2 at the ER-Golgi interface might be ideally suited for the physiological role of FAD2 in providing unsaturated membrane lipids for transport to other cellular membranes. While this physiological role of FAD2 has been considered a fact in previous reports, experimental evidence for the process is scarce. To address the influence of FAD2 on lipid unsaturation in a non-ER membrane, we used the phase-sensitive membrane dye, Di-4-ANEPPDHQ (Frescatada-Rosa et al., 2014; Roche et al., 2008) to analyze the effect of FAD2-mediated lipid unsaturation on the liquid phase ordered state of the plasma membrane, which is a membrane likely receiving unsaturated membrane lipids from the ER via the secretory pathway. Phase-sensitive fluorescent membrane dyes are inserted into cellular membranes and fluoresce only in the hydrophobic environment. Moreover, the fluorescent properties of the dye will change depending on the liquid-ordered state of the membrane, and thus the fluorescence spectra recorded in a given membrane can be used as a measure of its liquid-ordered state (Harris et al., 2002), indicated by a general polarization (GP) value (calculated as the difference between the fluorescence intensity for the ordered and disordered states divided by the sum of these intensities) (Frescatada-Rosa et al., 2014, Roche et al., 2008). Di-4-ANEPPDHQ was applied for 5 min to roots of Arabidopsis wild type controls and the *fad2-1* mutant, and fluorescence spectra were recorded. Figure 8(F) gives representative false-colored images representing the ensuing GP values (please refer to the color scale). The staining of controls and mutants was performed side-by-side. Please

note increased GP values for cell plates in both wild type controls and the *fad2-1* mutant (Figure 8F, lower panels), which verify previous findings (Frescatada-Rosa et al., 2014) and indicate successful analysis of liquid-ordered states. The quantitative analysis of GP values for plasma membranes (Figure 8G) indicates a significantly ($P < 0.01$) increased liquid phase order for the *fad2-1* mutant over that in wild type controls (each from 450 plasma membrane signals from 150 cells representing three independent biological experiments), consistent with a decrease in plasma membrane lipid unsaturation in the mutant. These data indicate an effect of the FAD2 enzyme on the lipid composition of the plasma membrane, likely in consequence of a distribution of lipid intermediates via ER and/or Golgi.

DISCUSSION

Metabolic pathways for plant fatty acid desaturation and lipid assembly have long been of interest in the context of industrial applications and seed oil biogenesis. Previous research indicates that the spatial distribution and the molecular interaction of the enzymes involved in the generation of modified fatty acids and the formation of seed oil are important factors to be considered for metabolic pathway engineering (Dyer & Mullen, 2001; McCartney et al., 2004). Therefore, we provide a detailed analysis of the subcellular distribution of FAD2, an example of a key player in plant fatty acid modification, using functional fluorescent fusion proteins, *in vivo* imaging, and quantitative image analysis. Our analyses of FAD2 localization in vegetative tissues show functional fluorescent fusions of FAD2 associated with pre-*cis*-Golgi stacks at ER-Golgi exit sites. The distinct pre-*cis*-Golgi-association of EYFP-FAD2 in the cells analyzed is consistent with the role of FAD2 in contributing to the control of membrane unsaturation in cellular membranes, which are physiologically linked by the secretory pathway. Some of the colocalization

The Plant Journal published by Society for Experimental Biology and John Wiley & Sons Ltd.,
*The Plant Journal*, (2024), **117**, 242–263

Figure 7. High-resolution imaging suggests a role for EYFP-FAD2 at pre-*cis*-Golgi stacks at ER-Golgi-exit sites. Golgi-association of EYFP-FAD2 was assessed in more detail relative to coexpressed markers decorating different *cis*-Golgi subcompartments. Images were acquired by SD microscopy (a, d) or by LSM (B, C).
(A) Median confocal sections of Arabidopsis mesophyll protoplasts coexpressing EYFP-FAD2 and the *cis*-Golgi marker, Man1-mC. Bottom left, Fluorescence intensity of EYFP-FAD2 and Man1-mC along the dashed line, as indicated. The detail image is a magnification from the dashed box in the merged image above, illustrating that EYFP-FAD2 fluorescence is omitted from the central areas of the structure decorated by the Man1-mC marker. White, overlapping EYFP and mCherry fluorescence. Scale, 10 μm.
(B) Median confocal sections of Arabidopsis mesophyll protoplasts coexpressing EYFP-FAD2 and the pre-*cis*-Golgi marker, MNS3-mC. Insets, Shape of the fluorescent particle highlighted by the arrowhead. The detail image is a magnification from the dashed box in the merged image, illustrating that EYFP-FAD2 fluorescence is omitted from the central areas of the structure decorated by the MNS3-mC marker. Face-on views and side views, as indicated, were selected from image sequences and illustrate the same organelle as it appeared in different frames. White, overlapping EYFP and mCherry fluorescence. Right panels, Fluorescence intensity of EYFP-FAD2 and MNS3-mC along the dashed line, as indicated. Black arrowheads indicate the lower fluorescence intensity in the center of the rings. Scale, 1 μm.
(C) Median confocal sections of Arabidopsis mesophyll protoplasts coexpressing EYFP-FAD2 and the pre-*cis*-Golgi marker, mC-Golgin-84A. Insets, Shape of the fluorescent particle highlighted by the arrowhead. The detail image is a magnification from the dashed box in the merged image, illustrating that ring-shaped EYFP-FAD2 fluorescence coincides with the ring-shaped distribution of the mC-Golgin-84A marker. Face-on views and side views, as indicated, were selected from image sequences and illustrate the same organelle as it appeared in different frames. White, overlapping EYFP and mCherry fluorescence. Scale, 1 μm. Right panels, Fluorescence intensity of EYFP-FAD2 and MNS3-mC along the dashed line, as indicated. Black arrowheads indicate the lower fluorescence intensity in the center of the rings.
(D) Relative localization of EYFP-FAD2 and ER-mC in mesophyll protoplasts analyzed by LSM. Left panels, Median confocal section of a protoplast cotransformed with EYFP-FAD2 and ER-mC. Computer-aided colocalization overlap analysis (right panels) highlights colocalizing pixels in false color (white) using the Fiji plugin 'Colocalization' with a ratio setting of 50 and an equal threshold setting of 10 for both the green and red channels, marking a ring-shaped overlap of ER and EYFP-FAD2, as indicated. Right panel, detailed image of detected overlap regions in the area indicated by the dashed box. Images are representative for 15 cells (A), 23 cells (B), 26 cells (C), or 24 cells (D), analyzed in 1 (A) or 5 (B, C) independent experiments.

experiments of FAD2 with various markers were performed using Arabidopsis mesophyll protoplasts. While protoplasts display increased rates of membrane trafficking and thus might display altered distribution patterns of enzymes relevant for relevant cellular processes, fluorescence distribution patterns observed for EYFP-FAD2 in Arabidopsis mesophyll protoplasts resembled those observed in root or leaf epidermal cells of stably transformed Arabidopsis (cf. Figures 4 and 5). Therefore, we conclude that the process of protoplastation did not impact our analysis.

Our analysis of the functional fluorescent markers in different cell types revealed association of fluorescent FAD2 fusions to pre-*cis*-Golgi stacks (Figures 4–8), and the FAD2 fusions did not decorate the entire Golgi but were restricted to a ring- or torus-shaped region between the ER and its exit to the Golgi cisternae (Figure 7). In face-on views, the Man1 or MNS3-markers appeared in flat, circular shapes with ~0.5–1 μm diameter (Nebenfuhr et al., 1999), whereas EYFP-FAD2 localized only to the rim of these circles. Nebenführ and coworkers have previously described ring-like structures for the Golgi marker GmMan1-GFP (Nebenfuhr et al., 1999; Nebenfuhr & Staehelin, 2001) and attributed this fluorescence distribution to osmotically collapsed Golgi stacks. Here, ring structures were only observed with EYFP-FAD2 and never for the Man1-GFP marker, so collapsed Golgi stacks do not seem to be the cause for the rings observed for EYFP-FAD2 (Figures 5–7). By contrast, the mC-Golgin-84A marker decorated ring-shaped structures that coincided with EYFP-FAD2 (Figure 7C), indicating that this marker might most closely resemble the distribution of EYFP-FAD2 at pre-*cis*-Golgi stacks. When imaging the side views of Golgi stacks (Figure 7A–C), the marker proteins and EYFP-FAD2 appeared as lines with a length of ~0.5–1 μm (Figure 7A),

equal to the diameter of the Golgi stacks in face-on views (Figure 7A), and structures in this transverse orientation allow to discern ER-proximal *cis*-Golgi and ER-averted *trans*-Golgi localization (Figure 6I). *cis*-Golgi and *trans*-Golgi signals have previously been distinguished by confocal microscopy (Saint-Jore-Dupas et al., 2006), and in the present study, fluorescence intensities of EYFP-FAD2 and the different Golgi-markers used coincided well in side-views of Golgi stacks, with close coincidence of fluorescence intensity of both fluorophores (Figures 6I and 7A–C). By contrast, the overlap for EYFP-FAD2 and a *trans*-Golgi marker was smaller (Figure 6I), suggesting that EYFP-FAD2 might localize preferentially to the peripheral region of the *cis*-face of Golgi stacks.

The Golgi-associated membrane region decorated by EYFP-FAD2 in immediate proximity to the ER (Figure 6A–D) was further defined by quantitative image analyses using the Fiji Plugin 'Colocalization'. These analyses show EYFP-FAD2-marked pre-*cis*-Golgi stacks surrounded by ER (Figure 7C), consistent with a general association of Golgi stacks with the ER. Boevink et al. (1998) previously found Golgi stacks in *Nicotiana clevelandii* leaf cells to move along the ER network on underlying actin cables, proposing that the moving Golgi stacks allowed the transfer of products (e.g. membrane lipids, proteins) from the ER to the *cis* site of Golgi stacks (Boevink et al., 1998). In light of this interpretation, the precise localization of EYFP-FAD2 at pre-*cis*-Golgi cisternae at ER-Golgi exit sites might similarly indicate a role for FAD2 in the transfer of modified fatty acids between ER and Golgi to facilitate distribution of unsaturated fatty acids via the secretory pathway. While this physiological role might require positioning of FAD2 in the proximity of the Golgi, the precise positioning of FAD2 at the pre-cis-Golgi might enable its dynamic
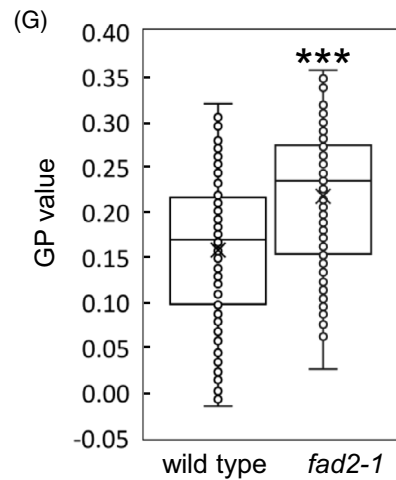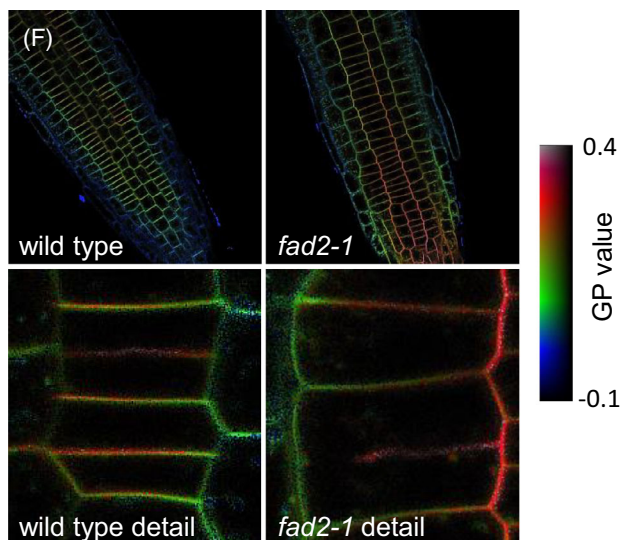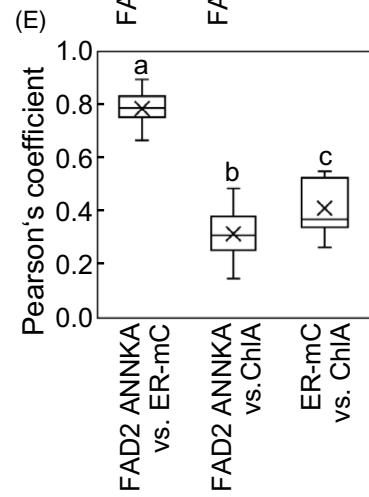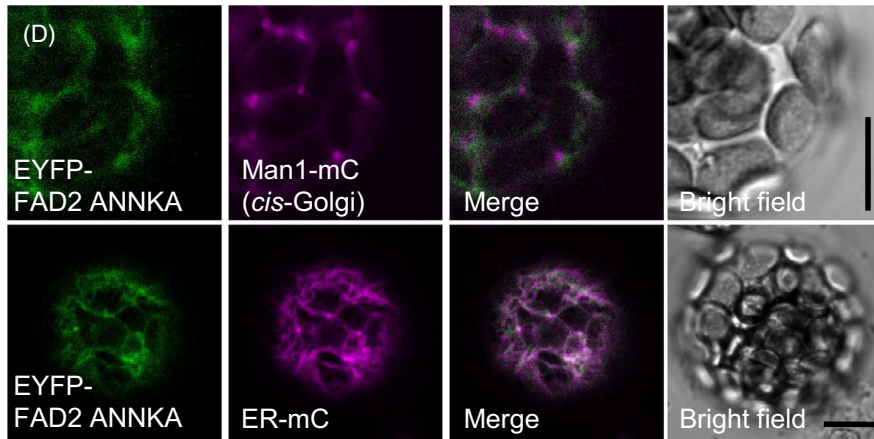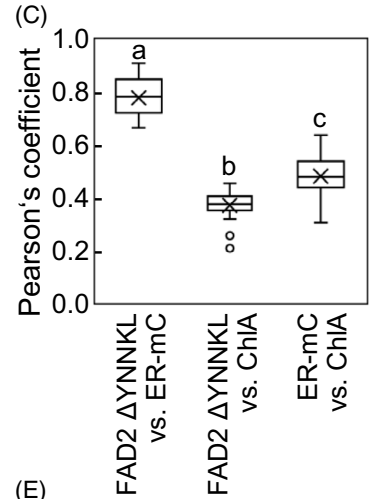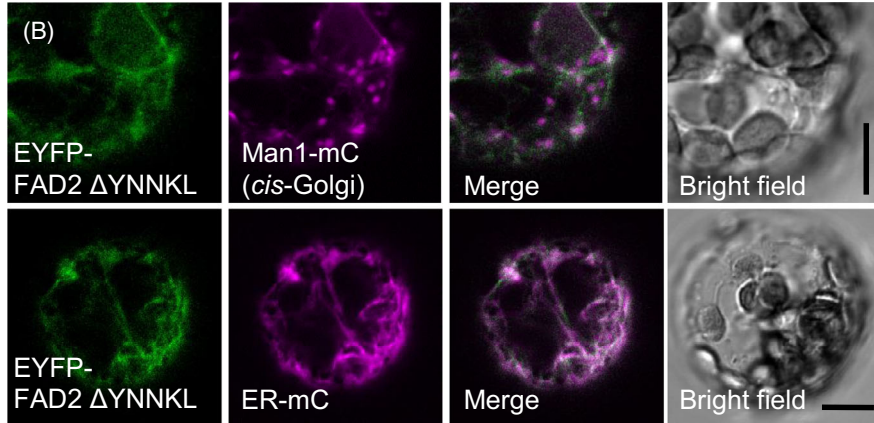
Figure 8. The C-terminal unusual retention sequence mediates precise localization of EYFP-FAD2.

The contribution of the unusual C-terminal retention sequence to the subcellular positioning of EYFP-FAD2 was analyzed by deleting or substituting critical C-terminal residues of the FAD2 sequence.

(A) Schematic overview of the variant FAD2 fusions used for analysis. Wild type FAD2 contains the C-terminal YNNKL motif previously described as critical for ER retention. In EYFP-FAD2 ΔYNNKL, this motif was deleted, whereas in the EYFP-FAD2 ANNKA variant, large hydrophobic amino acids were replaced by smaller alanine residues.

(B–E) Subcellular distribution of EYFP-FAD2 ΔYNNKL (B, C) or EYFP-FAD2 ANNKA (D, E), relative to coexpressed *cis*-Golgi-mC or ER-mC markers, as indicated. (C, E) PCCs for EYFP-FAD2 ΔYNNKL (C) or EYFP-FAD2 ANNKA (E) versus ER-mC, each calculated from eight z-stacks. Letters indicate significant differences ($P < 0.05$) according to a one-way ANOVA test with Tukey's post-hoc test.

(F, G) A role for FAD2 at the ER-Golgi transition was assessed by testing for an effect of the *fad2-1* mutation and ensuing reduction in membrane lipid unsaturation on plasma membrane nanostructure. Plasma membrane liquid phase order was visualized by staining with the phase-sensitive hydrophobic membrane dye, Di4-ANEPPDHQ. Roots of 7-days-old Arabidopsis wild type or *fad2-1* plants were stained side-by-side and fluorescence spectra were recorded. (F) False color images of the calculated GP values as an indication for membrane phase order. Upper panels, overview; lower panels, detail of meristematic/dividing cells, illustrating previously reported differences in membrane liquid phase order at the cell plate. (G) Quantitative analysis of plasma membrane GP values recorded for wild type controls and the *fad2-1* mutant, as indicated. Data represent 150 plasma membrane locations recorded in one experiment and are representative of three biological experiments with similar results. Asterisks indicate a significant difference according to a Student's *t*-test ($P < 0.001$).

redistribution within the ER towards sites where the enzyme might perform in a different context, such as oil biogenesis. In contrast to the close association of EYFP-FAD2 with pre-*cis*-Golgi stacks, other organellar markers did not colocalize with EYFP-FAD2, including markers for peroxisomes or oil bodies (Figure S4). This observation is in contrast to a known role of FAD2 and other enzymes of fatty acid metabolism in oil biogenesis at the ER. A possible explanation is that the location of FAD2 might change according to cellular requirements. The Arabidopsis root or leaf tissue for which we describe pre-*cis*-Golgi association of FAD2 represent parts of the plant that are not oleogenic, and it is possible that FAD2 displays a different subcellular distribution in tissues of seeds or siliques during seed filling and oil biogenesis. However, as oleogenic tissues are not easily accessible to high-resolution imaging, we currently cannot test FAD2 distribution under those conditions. FAD2, thus, might have alternative subcellular sites of action, possibly related to its physiological roles in different tissues and at different stages of plant development.

The FAD2 fusions used for our analysis were functional in yeast, as evident from the production of linoleic and hexadecadienoic acids upon expression of either EYFP-FAD2 or mC-FAD2. The overall lower amounts of dienoic products observed in yeast expressing the fluorescence-tagged FAD2-variants might be a consequence of differences in protein abundance between cells expressing the differently sized proteins, and thus influence the amount of fatty acid produced. However, the fatty acid patterns of the transgenic yeasts supported functionality of the fusion proteins, consistent with previous work by Kajiwara and coworkers also reporting the desaturation of $16:1^{\Delta 9}$ to $16:2^{\Delta 9,12}$ by FAD2 expressed in yeast (Kajiwara et al., 1996). As $16:1^{\Delta 9}$ present in yeast does not occur naturally in Arabidopsis, the ability of FAD2 to desaturate fatty acids with 16 carbon atoms illustrates the plasticity of fatty acid substrates accepted by desaturases depending on the metabolic context. Importantly, in Arabidopsis the expression of EYFP-FAD2 from an

intrinsic promoter fragment resulted in complementation of the *fad2-1* mutant regarding both fatty acid composition and macroscopic defects (Figures 2 and 3; Figure S1). The independent *fad2-1* EYFP-FAD2 lines all displayed significantly increased $18:2^{\Delta 9,12}$ in seed oil or in PC isolated from seedlings over that in the *fad2-1* mutant control, indicating functional complementation. The $18:2^{\Delta 9,12}$ levels in the complemented lines were only up to 85% of wild type levels and it cannot be ruled out that the EYFP-tag negatively influenced the functionality of the FAD2 fusion protein *in planta*, due to possible effects of the EYFP-tag on translation efficiency, protein stability or catalytic or physiological activity. However, with the complementation observed (Figures 2 and 3), such a negative effect - if at all present - must have been small. Overall, we found the fluorescence-tagged FAD2 variants to be active *in planta* and concluded that the fluorescence distribution of these markers might thus enable meaningful interpretation.

FAD2 contains a sequence motif at the extreme C-terminus (YNNKL), which has previously been characterized as sufficient to target small chimeric FAD2 protein fragments to the ER (McCartney et al., 2004). In that previous work, the addition or substitution of individual residues in this motif disrupted localization of the chimeric markers and resulted in their association with the plasma membrane (McCartney et al., 2004). By contrast, in the present study, full-length EYFP-FAD2 analyzed *in planta* was not ever observed at the plasma membrane, suggesting that the C-terminal localization sequence was unperturbed in the fusion proteins analyzed. McCartney et al. (2004) proposed that a localization of FAD2 to Golgi particles might reflect saturation of the retrograde transport machinery between ER and Golgi upon high expression levels of FAD2. In our experiments localization of FAD2 to pre-*cis*-Golgi stacks could dominate with hardly any fluorescence at the ER (e.g., Figure 4D), suggesting the pre-*cis*-Golgi cisternae as the actual target localization of FAD2 in the cells analyzed. Moreover, the C-terminal ER retention signal of FAD2 was found critical for the precise localization of full-

length EYFP-FAD2 (Figure 8), and its deletion resulted in protein variants that displayed a relaxed localization pattern still retained at the ER (Figure 8B–E). In fact, persisting ER retention of the FAD2 ΔYNNKL or FAD2 ANNKA variants indicates the presence of one or more further ER retention signals within the FAD2 sequence that have so far not been characterized. Moreover, as in previous work fluorescent fusions of short protein fragments with the YNNKL retention sequence of FAD2 displayed ER retention but no strict association with *cis*-Golgi particles (McCartney et al., 2004), it may follow that the precise positioning of FAD2 requires the coinciding action of several targeting signals. Combinations of an ER retention signal with such additional targeting signals may enable the FAD2 enzyme to associate with alternative ER subdomains, such as for instance the ER-Golgi transition or ER domains forming oil bodies, possibly controlled by posttranslational modifications, such as phosphorylation (Tang et al., 2005). However, such alternative and possibly dynamic redistribution of FAD2 is currently speculative based merely on known physiological roles of FAD2 in different cell types or at different stages of plant development. The observation that FAD2 variants with deleted or modified C-terminal targeting sequences no longer displayed physiological activity when expressed in yeast (Figure 8A–E) might indicate that the targeting sequence is relevant for enzyme function also in yeast; or that the modification or deletion of the respective sequence stretches has detrimental effects on the intrinsic protein folding and catalytic function of the enzyme. Based on the available data, this issue remains currently unresolved.

The observed localization at the ER-Golgi transition is likely linked to the physiological role of FAD2 in the cells or tissues analyzed. In previous studies, FAD2 has been mostly analyzed in the context of (seed) oil biogenesis. By contrast, cells of the root cortex or the leaf epidermis, as used in this study, do not accumulate high amounts of oil, and role and localization of FAD2 may thus differ. In the vegetative tissues studied, the increased degree of plasma membrane liquid phase order in the *fad2-1* mutant compared to wild type (Figure 8F,G) indicates that the FAD2 enzyme contributes substantially to the lipid composition and thus nano-organization of membranes that are not its primary site of residence. Since lipid assembly and fatty acid desaturation do not occur in all plant membranes, lipids are distributed from the ER to other endomembranes and the plasma membrane. A localization of FAD2 at the ER-Golgi transition places the enzyme at a central position for lipid distribution (Dupree & Sherrier, 1998; Park et al., 2021). As membrane lipid unsaturation is also involved in plant responses to a variety of stresses (He & Ding, 2020), the observed localization of FAD2 at pre-*cis*-Golgi cisternae is also consistent with its reported role in plant stress tolerance (Miquel & Browse, 1992; Nguyen et al., 2019; Wallis & Browse, 2002;

Zhang et al., 2012). Future experiments will be directed towards elucidating how FAD2 and possibly other enzymes of fatty acid modification may associate with different ER subdomains to perform their physiological function at different stages of development or under environmental challenges.

MATERIALS AND METHODS

Construction of plasmids

Plasmids for plant expression

The cDNA encoding FAD2 was amplified from Arabidopsis cDNA using the primer combination 5′-ATGCCTCGAGATGGGTGCAGG TGGAAGAAT-3′/5′-ATGCGCGGCCGCTCATAACTTATTGTTGTACC A-3′ and moved into the plasmid *pEntryA-pCaMV35S* as an *Xho*I/ *Not*I fragment. The cDNA encoding EYFP or mCherry was amplified using the primer combinations 5′-ATGCGGCGCGCCAT GGTGAGCAAGGGCGAGGA-3′/5′-ATGCCTCGAGCTTGTACAGC TCGTCCA-3′ or 5′-ATGCGGCGCGCCATGGTGAGCAAGGGCGAGG A-3′/5′-ATGCCTCGAGCTTGTACAGCTCGTCCA-3′, respectively, and moved in frame with the FAD2 insert into the same vector as *Asc*I/ *Xho*I fragments. For the expression of FAD2 from its endogenous promoter, the genomic sequence 2281 bp upstream of the start codon of the ATG was amplified and exchanged against the *pCaMV35S* promoter of *pEntryA-pCaMV35S* via *Sfi*I restriction sites. The cDNA encoding the ER-α-mannosidase I, MNS3, (Schoberer et al., 2019) was amplified from Arabidopsis cDNA using the primer combination 5′-ATGCGGCGCGCCATGTCGAAATCTCTACC ATA-3′/5′-ATGCCTCGAGGGTGTTTCTTCTTATTGGTAA-3′ and moved into the plasmid pEntryD-pCaMV35S as an *Asc*I/*Xho*I fragment. The cDNA encoding EYFP or mCherry was amplified using the primer combinations 5′-ATGCCTCGAGATGGTGAGCAAGGGCG AGGA-3′/5′-ATGCGGATCCCTTGTACAGCTCGTCCA-3′ or 5′-ATG CCTCGAGATGGTGAGCAAGGGCGAGGA-3′/5′-ATGCGGATCCCTT GTACAGCTCGTCCA-3′, respectively, and moved in frame with the MNS3 insert into the same vector as *Xho*I/*Bam*HI fragments.

The cDNA encoding the Arabidopsis Golgin-84A (Vieira et al., 2020) was amplified from Arabidopsis cDNA using the primer combination 5′-ATGCGGCGCGCCATGGCGTCTTGGCTT AAAGC-3′/5′-ATGCCTCGAGTTATAGTCTGAAAACGTTGTT-3′ and moved into the plasmid pEntryD-pCaMV35S as an *Asc*I/*Xho*I fragment. The cDNA encoding mCherry was amplified using the primer combination 5′-ATGCGTCGACATGGTGAGCAAGGGCG AGGA-3′/5′-ATGCGGCGCGCCACTTGTACAGCTCGTCCA-3′ and moved in frame with the Golgin-84A insert into the same vector as *Sal*I/*Asc*I fragment.

Plasmids for yeast expression

The FAD2 cDNA was amplified from *pEntryA-pCaMV35S* using the primer combination 5′-ATGCGAATTCATGGGTGCAGGTGGAAGAA T-3′/5′-ATGCGCGGCCGCTCATAACTTATTGTTGTACCA-3′ and moved as an *EcoR*I/*Not*I fragment into the plasmid *pESC-TRP*. The cDNA for EYFP-FAD2 or mCherry-FAD2 were amplified from the respective pEntry plasmids using the primer combinations 5′-ATGC GAATTCATGGTGAGCAAGGGCGAGGA-3′/5′-ATGCGCGGCCGC TCATAACTTATTGTTGTACCA-3′ or 5′-ATGCGAATTCATGGTGAG CAAGGGCGAGGA-3′/5′-ATGCGGCGGCCGCTCATAACTTATTGTTGT ACCA-3′, respectively, and moved into *pESC-TRP* as *EcoR*I/*Not*I fragments. Plasmids encoding organelle markers used in this study were elements of the multi-color set of *in vivo* organelle markers (Nelson et al., 2007).

Plant material and growth conditions

Plant experiments were conducted using *A. thaliana* ecotype Columbia-0 (wild type). The Arabidopsis *fad2-1* mutant (Lemieux et al., 1990; Okuley et al., 1994) was obtained from NASC. The *GFP-HDEL* ER marker line was a gift from Prof. Dr. Staffan Persson, University of Copenhagen, DK. Plants used for protoplast isolation were grown on soil (Substrate 1, Klasmann-Deilmann GmbH, Geeste, Germany, with one part of vermiculite) under short-day conditions (8–10 h light at 21°C, 14–16 h dark at 18°C) for 6–8 weeks. Plants for stable transformation and seed propagation were grown for 4–6 weeks under short-day conditions, followed by 2 weeks of long-day conditions (16 h light at 21°C, 8 h darkness at 18°C) to induce shoot growth. For growth on solid ½ MS medium (0.22% [w/v] Murashige and Skoog medium incl. Modified vitamins [Duchefa], 1% [w/v] sucrose, pH 5.6), seeds were surface sterilized with sodium-hypochlorite solution with 0.01% (v/v) Triton-X-100, stratified for 2 days at 4 °C in the dark, and grown under long-day conditions.

Plant transformation and genotyping

Arabidopsis plants were transformed by floral dipping (Clough & Bent, 1998) using *Agrobacterium tumefaciens* AGL-0 (Lazo et al., 1991) and 0.05% (v/v) Silwet L-77 as a surfactant. T1 seeds were harvested, grown on soil under short-day conditions until four true leaves were formed, and transformants were selected by exposure to 0.045% (v/v) Basta (glufosinate ammonium; Bayer, Leverkusen, Germany). T2 seeds were harvested and used for experiments and propagation.

Plant salt treatment

Plants for salt stress experiments were grown for 7 days under long-day conditions on ½ MS medium containing 0 mM (control), 75 mM, 100 mM, or 125 mM NaCl. Plates were scanned and root lengths were determined using Fiji (Schindelin et al., 2012).

Yeast material and growth

Yeast (*Saccharomyces cerevisiae* INVSc1; Invitrogen, Thermo Fisher Scientific, Schwerte, Germany) was grown at 30°C in liquid YPAD media (1% [w/v] yeast extract, 2% [w/v] peptone, 0.004% [w/v] adenine hemi sulfate, 2% [w/v] glucose). Yeast cells were transformed with the LiAc/PEG method (Ito et al., 1983). Transformed yeast was grown on SD medium containing 0.17% (w/v) yeast nitrogen base, 0.5% (w/v) $(NH_4)_2SO_4$, 2% (w/v) micro-agar, 2% (w/v) glucose or galactose, and a mixture of amino acids/nucleoside precursors. For selection, the relevant amino acids were omitted. For transgene expression cultures were grown for 3–4 days at 20°C in the presence of 2% (w/v) galactose. For analysis, 20 OD-units were harvested by centrifugation at 2500 *g* for 5 min, washed once in 5 ml of TE buffer (10 mM Tris, 1 mM EDTA, pH 7.5) and pellets were frozen in liquid nitrogen and stored at −20°C until analysis.

Analysis of lipids and fatty acids

Extraction and derivatization of yeast fatty acids

Sedimented cells were resuspended in 2 ml FAME solution (2.75% (v/v) H_2SO_4 and 2% (v/v) dimethoxypropane in methanol) for transmethylation (Miquel & Browse, 1992). For fatty acid quantification, 50 μg tripentadecanoin was added to each sample as an internal standard. The reaction was incubated at 80°C for 1 h. The formed FAMEs were extracted with 200 μl of 5 M NaCl and 2 ml

n-hexane. The n-hexane phases were evaporated under air stream and FAMEs were redissolved in 100 μl acetonitrile for GC analysis.

Extraction and derivatization of Arabidopsis seed fatty acids

FAMEs were prepared from single Arabidopsis seeds by trans-esterification with 10 μl of 0.2 M trimethyl sulfonium hydroxide (Butte et al., 1982). The resulting FAMEs were dissolved in 10 μl acetonitrile and analyzed with GC.

Lipid extraction

Total lipids were extracted using the Bligh-Dyer method (Bligh & Dyer, 1959) from 14-day-old Arabidopsis seedlings grown on ½ MS-medium. In brief, grounded plant material was mixed with chloroform:methanol (2:1, v/v) and extracted with chloroform and H_2O to achieve a final ratio of chloroform:methanol:H_2O of 2:2:2, (v/v/v). The organic phases were dried under air stream and the remaining lipids were dissolved in 1 ml of chloroform. For lipid class separation the solid phase adsorption chromatography was used. Neutral lipids, galactolipids, and phospholipids were separated on silica solid phase extraction columns with a capacity for 100 mg starting material (HF Bond Elut 1CC LRC-SI, 100 mg; Agilent Technologies, VWR International GmbH, Darmstadt, Germany) as previously described (Launhardt et al., 2021). The lipid fractions were dissolved in 100 μl chloroform and subjected to thin-layer chromatography (TLC).

Separation of lipid classes by TLC

To separate lipids from phospholipid and glycolipid fractions from seedlings, samples were spotted onto silica gel plates (TLC silica gel plates 60, 20 × 20 cm, glass supported; Merck, Darmstadt, Germany). Authentic standards (5 μg) were used for identification (Avanti). TLC plates were developed in glass chambers using acetone:toluene:H_2O, 90:30:7 (v/v/v) for glycolipids or chloroform:methanol:acetic acid, 65:25:8 (v/v/v) for phospholipids. To determine the fatty acid composition of individual lipid species, lipids were scraped off TLC plates and FAMEs were prepared by trans-esterification with sodium methoxide (Launhardt et al., 2021). As internal standard 10 μg tripentadecanoin was added to each sample. The FAMEs were dissolved in 100 μl acetonitrile and analyzed by GC.

Analysis of FAMEs by gas chromatography (GC-FID)

The analysis of FAMEs was performed as previously described (Launhardt et al., 2021) using a GC-2010Plus (Shimadzu Deutschland GmbH, Duisburg, Germany) coupled with a flame ionization detector and a DB-23 column (30 m × 0.25 mm; 0.25 μm coating thickness; Agilent Technologies). Helium was used as carrier gas and samples were injected at 220°C, and chromatography was performed using a temperature gradient raising the oven temperature after 1 min at 150–200°C at a rate of 25°C min^{-1}, followed by an increase to 250°C at a rate of 4°C/min and remaining at 250°C for 6 min. The data were analyzed using the GC Solution software (version 2.31.00; Shimadzu Deutschland GmbH) and FAMEs were identified by comparison with appropriate reference substances.

Generation and transformation of mesophyll protoplasts

Mesophyll protoplast preparation from 6- to 8-week-old Arabidopsis leaves and transformation were done as previously described (Yoo et al., 2007). Transformed protoplasts were incubated overnight in the dark at 20°C and were used for microscopic analyses or harvested for immunodetection.

Immunodetection

Immunodetection was performed as previously described (Menzel et al., 2019). Goat anti-mCherry antiserum (#AB0040-200; Sicgen, Cantanhede, Portugal) was diluted 1:2500 in 3% (w/v) milk powder in TBS (50 mM Tris–HCl pH 7.5, 150 mM NaCl) according to the manufacturer's instructions. The secondary rabbit anti-goat antiserum (#A4187; Sigma-Aldrich, Darmstadt, Germany) was diluted 1:30 000 in 3% (w/v) milk powder in TBS. Proteins were detected using bromochloroindoyl phosphate/nitro blue tetrazolium in alkaline phosphatase buffer (100 mM Tris–HCl pH 9.5, 100 mM NaCl, 5 mM $MgCl_2$).

Live cell microscopy and image processing

Images were acquired either with a Zeiss Lightsheet Z1 microscope, a Zeiss LSM880 Airyscan FAST system, or with a Zeiss Cell observer SD with a Yokogawa CSU-X1 spinning disc unit (all from Carl-Zeiss GmbH, Jena, Germany). Light sheet microscopy was performed to image mostly unperturbed intact roots as previously described (Flood et al., 2013; Maizel et al., 2011). Briefly, 1-week-old seedlings grown on plates were transferred into a syringe containing 1% low-melting agarose supplied with ½ MS medium and 1% sucrose. The syringe was introduced into the sample chamber containing in ½ MS-medium with 1% sucrose. YFP fluorescence was recorded using an excitation of 488 nm light and a detection range of 505–545 nm. Multistacks were obtained using z-sections of 0.42 μm thickness covering the complete root in time intervals of 6 min over 2 h. Image acquisition was done with ZEN Black for lightsheet, whereas rendering was performed using arivis vision 4D (Zeiss). For imaging of Arabidopsis mesophyll protoplasts, an LSM880 Airyscan FAST system (Carl Zeiss, Jena, Germany) with a Plan-Apochromat 40×/0.95 Korr M27 objective was used. Seedlings were imaged using a 63× oil immersion objective (Plan-Apochromat 63×/1.4 Oil DIC M27; Carl Zeiss). During acquisition with the LSM880, EYFP was excited at 514 nm and imaged with an HFT 514 nm major beam splitter (MBS) and recorded at 520–570 nm while mCherry was excited at 561 nm and imaged with an HFT 561 nm MBS and recorded at 580–630 nm. Chlorophyll A was excited at 633 nm and recorded at 650–720 nm. The pinhole was kept at ~1 Airy unit. Z-stacks covering the cell from one edge to the center were generated with 0.5–1 μm between each frame, resulting in ~20–30 frames per cell. Images were acquired with an 8-bit bit depth using ZEN Black image analysis software (version 14.0.18.201; Carl Zeiss). A Zeiss Cell Observer spinning disc microscope was used for fast acquisition of highly mobile EYFP or mCherry signals. Images were acquired with a 63× oil immersion objective and recorded with a Photometrics Evolve 512 Delta EM-CCD camera. EYFP was excited at 491 nm and mCherry at 561 nm using a multichannel dichroic and an ET525/50M or an ET595/50M band pass emission filter (Chroma Technology, Olching, Germany) for EYFP and mCherry, respectively, and using Zen Blue image analysis software.

Application of dyes

Five-day-old wild type (Col-0) or *fad2-1* seedlings were incubated in 5 μM Di-4-ANEPPDHQ (Invitrogen, Thermo Fisher Scientific) in liquid ½ MS medium for 5 min and washed with pure ½ MS medium, root tips were placed on microscopic slides mounted in liquid ½ MS and examined with an LSM880 equipped with a 40× water immersion objective. Di-4-ANEPPDHQ was excited at 488 nm and fluorescence was detected at 499–580 nm and 619–750 nm. Images were taken within the root elongation zone. All images were processed with Fiji/ImageJ software (Schindelin

et al., 2012) using the macro to generate GP images and to calculate GP values (Owen et al., 2011).

Quantitative image analysis

Image processing was performed using the software ImageJ Fiji (version 1.51; Schindelin et al., 2012). Images were contrast-enhanced with a maximum of 0.1% saturated pixels. Z-projections from z-stacks were generated using the projection type 'maximum intensity'. Leaf areas from complemented plant lines were calculated using the Fiji plugin simple interactive object extraction (SIOX). Pearson's correlation coefficients (PCC) were determined using the Fiji-plugin Just Another Colocalization Plugin (JACoP) (Bolte & Cordelieres, 2006) based on unprocessed z-stack images of up to 512 × 512 pixels. Line intensity plots were generated using Fiji and illustrated with the plugin 'dotted line'. To highlight colocalized areas, the Fiji plugin 'Colocalization' was used based on LSM z-stacks as input. During image acquisition, care was taken that acquisition settings were identical for all cells and samples.

Statistics

Bar charts and box plots were generated using Microsoft Office 365 (Microsoft Corporation, Redmond, WA, USA). Error bars in bar charts represent the sample standard deviation. The box plots depict the inner quartiles with the whiskers indicating the maximum and minimum. Values 1.5 times larger or smaller than the interquartile range are regarded as outliers. Outliers are represented by circles. The cross marks the mean, and the line in between the quartiles marks the median. Statistical significance was determined using one-way ANOVA with a subsequent Tukey's *post hoc* test (significance level $P < 0.05$). Statistical analyses were performed using the online tool 'Statistics Kingdom' (www.statskingdom.com).

ACCESSION NUMBERS

Arabidopsis FAD2, At3g12120; Arabidopsis Golgin-84A, At2g19950; Arabidopsis MNS3, At1g30000.

CONFLICT OF INTEREST STATEMENT

The authors declare no conflicts of interest.

SUPPORTING INFORMATION

Additional Supporting Information may be found in the online version of this article.

Figure S1. Ectopic expression of EYFP-FAD2 increases salt tolerance in the Arabidopsis *fad2-1* mutant. The functionality of the

EYFP-FAD2 fusion was assessed by testing for complementation of the salt intolerance displayed by the Arabidopsis *fad2-1* mutant. (A) Plants were grown on vertical plates of ½ MS medium containing the indicated amount of NaCl for 7 days under long-day conditions (16 h light, 8 h dark) after 2 days of stratification. (B) Root lengths were measured, and the relative root length compared to mock-treated plants is shown in the bar chart. Data represent mean ± standard deviation. Significant differences were determined using one-way ANOVA with a Tukey's *post-hoc* test ($P < 0.05$) for each salt concentration. Letters indicate significantly different categories of samples. The experiments were performed with 12 to 19 seedlings per line and salt concentration.

Figure S2. Immunodetection of mCherry-FAD2 in Arabidopsis mesophyll protoplasts. The integrity of mCherry-FAD2 fusions expressed in Arabidopsis mesophyll protoplasts was analyzed in protein extracts by immunodetection using an antiserum against mCherry. Left, Protein molecular weight standard, as indicated (M); right, calculated sizes of the fusion proteins analyzed. mCherry-FAD2 fusion proteins of the correct sizes were detected in protoplasts with expression driven by an intrinsic promoter fragment (as used in all experiments shown in this study) as well as in protoplasts expressing the fusions under control of the cauliflower mosaic virus 35S promoter, as indicated.

Figure S3. Calibration of colocalization analyses using different combinations of organellar markers. The recording of colocalization events by our microscopic setup was tested by comparing the relative fluorescence distributions of coexpressed markers carrying different fluorescence tags. All markers were imaged by LSM upon coexpression in Arabidopsis mesophyll protoplasts. (A) Representative merged fluorescence images of the marker combinations ER-GFP and ER-mC (shown as a maximum intensity projection of a z-stack of 24 optical sections with ~0.6 μm distance); ER-mC and the *cis*-Golgi marker Man1-EYFP; the pre-cis-Golgi marker MNS3-mC and MNS3-EYFP; and the cis-Golgi marker Man1-MC and the trans-Golgi marker ST-EYFP, as indicated. White indicates colocalization in the markers. Scale, 5 μm. (B) PCCs indicating the degree of colocalization calculated from eight cells (ER-GFP versus ER-mC); 15 cells (ER-mC versus Man1-EYFP); 23 cells (MNS3-mC versus MNS3-EYFP); and 22 cells (Man1-MC versus ST-EYFP).

Figure S4. EYFP-FAD2 does not coincide with fluorescent markers for oil bodies or peroxisomes. Arabidopsis mesophyll protoplasts were cotransformed with *pEntryA-pFAD2::EYFP-FAD2* and either the peroxisome marker construct *pEntryD-pCaMV35S::CFP-SKL* (A–C) or the oil body marker construct *pCAMBIA3300.0GS-pCaMV35S::OLE3-mCherry* (D–F). z-Stacks covering the cell from one edge to the center with ~0.6 μm distance between the optical sections were generated by LSM. EYFP-FAD2 fluorescence is depicted in green and the respective organelle markers in magenta. Scale, 10 μm. Letters indicate categories of significantly different samples according to a one-way ANOVA test with Tukey's *post-hoc* test ($p < 0.05$). (A) Coexpression of EYFP-FAD2 with a peroxisome marker (CFP-SKL). A single confocal slice is shown. The detail image (right) represents a merged image from a single confocal plane. (B) Pearson's correlation coefficients (PCCs) between EYFP-FAD2 and the peroxisomal marker or chlorophyll A (ChlA) were calculated based on 10 z-stacks acquired by LSM. (C) Intensity profile for EYFP-FAD2 (green) and the peroxisome-marker (magenta) along the line highlighted in the left panels. (D) Coexpression of EYFP-FAD2 with OLE3-mCherry (oil body marker). A maximum intensity z-projection is shown. The detail image (right) represents a merged image from a single confocal plane. Scale, 10 μm. (E) PCCs between EYFP-FAD2 and the OLE3-mCherry or ChlA were calculated based on 33 z-stacks from three

independent experiments acquired by LSM. Data on MNS3-mC versus MNS3-EYFP were included as a positive control for the correlation analysis. (F) Intensity profile for EYFP-FAD2 (green) and the oil body marker (magenta) along the line highlighted in the left panels. Images are representative of one (A–C) or three (D–F) independent experiments using a total of 10 (A–C) or 33 (D–F) cells.

Figure S5. The physiological function of the EYFP-FAD2 ΔYNNKL or EYFP-FAD2 ANNKA variants was assessed by heterologous expression in yeast and biochemical analysis. Expression of EYFP-FAD2 or an empty vector served as control. (A) Microscopic appearance of the transgenic yeast displaying substantial EYFP fluorescence. Scales, 5 μm. (B) GC-FID analysis of $16:2^{\Delta 9,12}$ and $18:2^{\Delta 9,12}$ formed in the transgenic yeast from endogenous substrates. Conversion was only detected for the EYFP-FAD2 control. n.d., not detected. Data represent mean ± standard deviation from three independent experiments.

REFERENCES

Bligh, E.G. & **Dyer, W.J.** (1959) A rapid method of total lipid extraction and purification. *Canadian Journal of Biochemistry and Physiology*, **37**, 911–917.

Boevink, P., **Oparka, K.**, **Santa Cruz, S.**, **Martin, B.**, **Betteridge, A.** & **Hawes, C.** (1998) Stacks on tracks: the plant Golgi apparatus traffics on an actin/ER network. *The Plant Journal*, **15**, 441–447.

Bolte, S. & **Cordelieres, F.P.** (2006) A guided tour into subcellular colocalization analysis in light microscopy. *Journal of Microscopy*, **224**, 213–232.

Broadwater, J.A., **Whittle, E.** & **Shanklin, J.** (2002) Desaturation and hydroxylation. Residues 148 and 324 of Arabidopsis FAD2, in addition to substrate chain length, exert a major influence in partitioning of catalytic specificity. *The Journal of Biological Chemistry*, **277**, 15613–15620.

Browse, J., **McConn, M.**, **James, D., Jr.** & **Miquel, M.** (1993) Mutants of Arabidopsis deficient in the synthesis of alpha-linolenate. Biochemical and genetic characterization of the endoplasmic reticulum linoleoyl desaturase. *Journal of Biological Chemistry*, **268**, 16345–16351.

Butte, W., **Eilers, J.** & **Kirsch, M.** (1982) Trialkylsulfonium- and trialkylselenoniumhydroxides for the pyrolytic alkylation of acidic compounds. *Analytical Letters*, **15**, 841–850.

Cahoon, E.B., **Lindqvist, Y.**, **Schneider, G.** & **Shanklin, J.** (1997) Redesign of soluble fatty acid desaturases from plants for altered substrate specificity and double bond position. *Proceedings of the National Academy of Sciences of the United States of America*, **94**, 4872–4877.

Clough, S.J. & **Bent, A.F.** (1998) Floral dip: a simplified method for *Agrobacterium*-mediated transformation of *Arabidopsis thaliana*. *The Plant Journal*, **16**, 735–743.

Dupree, P. & **Sherrier, D.J.** (1998) The plant Golgi apparatus. *Biochimica et Biophysica Acta*, **1404**, 259–270.

Dyer, J.M. & **Mullen, R.T.** (2001) Immunocytological localization of two plant fatty acid desaturases in the endoplasmic reticulum. *FEBS Letters*, **494**, 44–47.

Flood, P.M., **Kelly, R.**, **Gutiérrez-Heredia, L.** & **Reynaud, E.G.** (2013) *Zeiss Light Sheet Z1 – sample preparation* [white paper]. Harvard Center for Biological Imaging, Harvard University. Available from: https://hcbi.fas.harvard.edu/files/lightsheetz1_sample-preparation_zeiss.pdf

Frescatada-Rosa, M., **Stanislas, T.**, **Backues, S.K.**, **Reichardt, I.**, **Men, S.**, **Boutte, Y.** *et al.* (2014) High lipid order of Arabidopsis cell-plate membranes mediated by sterol and DYNAMIN-RELATED PROTEIN1A function. *The Plant Journal*, **80**, 745–757.

Harris, F.M., **Best, K.B.** & **Bell, J.D.** (2002) Use of laurdan fluorescence intensity and polarization to distinguish between changes in membrane fluidity and phospholipid order. *Biochimica et Biophysica Acta*, **1565**, 123–128.

He, M. & **Ding, N.Z.** (2020) Plant unsaturated fatty acids: multiple roles in stress response. *Frontiers in Plant Science*, **11**, 562785.

Heilmann, I., **Pidkowich, M.S.**, **Girke, T.** & **Shanklin, J.** (2004) Switching desaturase enzyme specificity by alternate subcellular targeting. *Proceedings of the National Academy of Sciences of the United States of America*, **101**, 10266–10271.

Heilmann, M., **Iven, T.**, **Ahmann, K.**, **Hornung, E.**, **Stymne, S.** & **Feussner, I.** (2012) Production of wax esters in plant seed oils by oleosomal cotargeting of biosynthetic enzymes. *Journal of Lipid Research*, **53**, 2153–2161.

Horton, H.R., Moran, L.A., Scrimgeour, K.G., Perry, M.D. & Rawn, J.D. (2006) Lipids and membranes. In: Carlson, G. (Ed.) *Principles of biochemistry*. Pearson Prentice Hall: Upper Saddle River, NJ, pp. 253–292.

Ito, H., Fukuda, Y., Murata, K. & Kimura, A. (1983) Transformation of intact yeast cells treated with alkali cations. *Journal of Bacteriology*, 153, 163–168.

Kajiwara, S., Shirai, A., Fujii, T., Toguri, T., Nakamura, K. & Ohtaguchi, K. (1996) Polyunsaturated fatty acid biosynthesis in *Saccharomyces cerevisiae*: expression of ethanol tolerance and the FAD2 gene from *Arabidopsis thaliana*. *Applied and Environmental Microbiology*, 62, 4309–4313.

Launhardt, L., Matzner, M., Heilmann, M. & Heilmann, I. (2021) Analysis of phosphoinositides from complex plant samples by solid-phase adsorption chromatography and subsequent quantification via thin-layer and gas chromatography. *Methods in Molecular Biology*, 2295, 379–389.

Lazo, G.R., Stein, P.A. & Ludwig, R.A. (1991) A DNA transformation-competent Arabidopsis genomic library in *Agrobacterium*. *Biotechnology (N Y)*, 9, 963–967.

Lee, M.W., Padilla, C.S., Gupta, C., Galla, A., Pereira, A., Li, J. *et al.* (2020) The FATTY ACID DESATURASE2 family in tomato contributes to primary metabolism and stress responses. *Plant Physiology*, 182, 1083–1099.

Lemieux, B., Miquel, M., Somerville, C. & Browse, J. (1990) Mutants of Arabidopsis with alterations in seed lipid fatty acid composition. *Theoretical and Applied Genetics*, 80, 234–240.

Lou, Y., Schwender, J. & Shanklin, J. (2014) FAD2 and FAD3 desaturases form heterodimers that facilitate metabolic channeling in vivo. *The Journal of Biological Chemistry*, 289, 17996–18007.

Maizel, A., von Wangenheim, D., Federici, F., Haseloff, J. & Stelzer, E.H. (2011) High-resolution live imaging of plant growth in near physiological bright conditions using light sheet fluorescence microscopy. *The Plant Journal*, 68, 377–385.

McCartney, A.W., Dyer, J.M., Dhanoa, P.K., Kim, P.K., Andrews, D.W., McNew, J.A. *et al.* (2004) Membrane-bound fatty acid desaturases are inserted co-translationally into the ER and contain different ER retrieval motifs at their carboxy termini. *The Plant Journal*, 37, 156–173.

Meesapyodsuk, D., Reed, D.W., Covello, P.S. & Qiu, X. (2007) Primary structure, regioselectivity, and evolution of the membrane-bound fatty acid desaturases of *Claviceps purpurea*. *The Journal of Biological Chemistry*, 282, 20191–20199.

Menzel, W., Stenzel, I., Helbig, L.M., Krishnamoorthy, P., Neumann, S., Eschen-Lippold, L. *et al.* (2019) A PAMP-triggered MAPK cascade inhibits phosphatidylinositol 4,5-bisphosphate production by PIP5K6 in *Arabidopsis thaliana*. *The New Phytologist*, 224, 833–847.

Miquel, M. & Browse, J. (1992) Arabidopsis mutants deficient in polyunsaturated fatty acid synthesis. Biochemical and genetic characterization of a plant oleoyl-phosphatidylcholine desaturase. *Journal of Biological Chemistry*, 267, 1502–1509.

Nebenfuhr, A., Gallagher, L.A., Dunahay, T.G., Frohlick, J.A., Mazurkiewicz, A.M., Meehl, J.B. *et al.* (1999) Stop-and-go movements of plant Golgi stacks are mediated by the acto-myosin system. *Plant Physiology*, 121, 1127–1142.

Nebenfuhr, A. & Staehelin, L.A. (2001) Mobile factories: Golgi dynamics in plant cells. *Trends in Plant Science*, 6, 160–167.

Nelson, B.K., Cai, X. & Nebenfuhr, A. (2007) A multicolored set of in vivo organelle markers for co-localization studies in Arabidopsis and other plants. *The Plant Journal*, 51, 1126–1136.

Nguyen, V.C., Nakamura, Y. & Kanehara, K. (2019) Membrane lipid polyunsaturation mediated by FATTY ACID DESATURASE 2 (FAD2) is involved in endoplasmic reticulum stress tolerance in *Arabidopsis thaliana*. *The Plant Journal*, 99, 478–493.

Okuley, J., Lightner, J., Feldmann, K., Yadav, N., Lark, E. & Browse, J. (1994) Arabidopsis FAD2 gene encodes the enzyme that is essential for polyunsaturated lipid synthesis. *Plant Cell*, 6, 147–158.

Owen, D.M., Rentero, C., Magenau, A., Abu-Siniyeh, A. & Gaus, K. (2011) Quantitative imaging of membrane lipid order in cells and organisms. *Nature Protocols*, 7, 24–35.

Park, K., Ju, S., Kim, N. & Park, S.Y. (2021) The Golgi complex: a hub of the secretory pathway. *BMB Reports*, 54, 246–252.

Pidkowich, M.S., Nguyen, H.T., Heilmann, I., Ischebeck, T. & Shanklin, J. (2007) Modulating seed beta-ketoacyl-acyl carrier protein synthase II level converts the composition of a temperate seed oil to that of a palm-like tropical oil. *Proceedings of the National Academy of Sciences of the United States of America*, 104, 4742–4747.

Roche, Y., Gerbeau-Pissot, P., Buhot, B., Thomas, D., Bonneau, L., Gresti, J. *et al.* (2008) Depletion of phytosterols from the plant plasma membrane provides evidence for disruption of lipid rafts. *The FASEB Journal*, 22, 3980–3991.

Saint-Jore-Dupas, C., Nebenfuhr, A., Boulaflous, A., Follet-Gueye, M.L., Plasson, C., Hawes, C. *et al.* (2006) Plant N-glycan processing enzymes employ different targeting mechanisms for their spatial arrangement along the secretory pathway. *Plant Cell*, 18, 3182–3200.

Schindelin, J., Arganda-Carreras, I., Frise, E., Kaynig, V., Longair, M., Pietzsch, T. *et al.* (2012) Fiji: an open-source platform for biological-image analysis. *Nature Methods*, 9, 676–682.

Schoberer, J., Konig, J., Veit, C., Vavra, U., Liebminger, E., Botchway, S.W. *et al.* (2019) A signal motif retains Arabidopsis ER-alpha-mannosidase I in the cis-Golgi and prevents enhanced glycoprotein ERAD. *Nature Communications*, 10, 3701.

Shanklin, J. & Cahoon, E.B. (1998) Desaturation and related modifications of fatty acids. *Annual Review of Plant Physiology and Plant Molecular Biology*, 49, 611–641.

Shanklin, J., Whittle, E. & Fox, B.G. (1994) Eight histidine residues are catalytically essential in a membrane-associated iron enzyme, stearoyl-CoA desaturase, and are conserved in alkane hydroxylase and xylene monooxygenase. *Biochemistry*, 33, 12787–12794.

Somerville, C., Browse, J., Jaworski, J.G. & Ohlrogge, J.B. (2000) Lipids. In: Buchanan, B.B., Gruissem, W. & Jones, R.L. (Eds.) *Biochemistry and molecular biology of plants*. Rockville, MD: American Society of Plant Physiologists, pp. 456–526.

Stellmach, H., Hose, R., Rade, A., Marillonnet, S. & Hause, B. (2022) A new set of golden-gate-based organelle marker plasmids for colocalization studies in plants. *Plants (Basel)*, 11, 2620.

Tang, G.Q., Novitzky, W.P., Carol Griffin, H., Huber, S.C. & Dewey, R.E. (2005) Oleate desaturase enzymes of soybean: evidence of regulation through differential stability and phosphorylation. *The Plant Journal*, 44, 433–446.

Vieira, V., Pain, C., Wojcik, S., Spatola Rossi, T., Denecke, J., Osterrieder, A. *et al.* (2020) Living on the edge: the role of Atgolgin-84A at the plant ER-Golgi interface. *Journal of Microscopy*, 280, 158–173.

Wallis, J.G. & Browse, J. (2002) Mutants of Arabidopsis reveal many roles for membrane lipids. *Progress in Lipid Research*, 41, 254–278.

Wee, E.G., Sherrier, D.J., Prime, T.A. & Dupree, P. (1998) Targeting of active sialyltransferase to the plant Golgi apparatus. *Plant Cell*, 10, 1759–1768.

Yamada, K., Hara-Nishimura, I. & Nishimura, M. (2011) Unique defense strategy by the endoplasmic reticulum body in plants. *Plant & Cell Physiology*, 52, 2039–2049.

Yoo, S.D., Cho, Y.H. & Sheen, J. (2007) Arabidopsis mesophyll protoplasts: a versatile cell system for transient gene expression analysis. *Nature Protocols*, 2, 1565–1572.

Zhang, J., Liu, H., Sun, J., Li, B., Zhu, Q., Chen, S. *et al.* (2012) Arabidopsis fatty acid desaturase FAD2 is required for salt tolerance during seed germination and early seedling growth. *PLoS One*, 7, e30355.